Impact of dust addition on Mediterranean plankton communities under present and future conditions of pH and temperature: an experimental overview

Frédéric Gazeau[1], Céline Ridame[2], France Van Wambeke[3], Samir Alliouane[1], Christian Stolpe[1], Jean-Olivier Irisson[1], Sophie Marro[1], Jean-Michel Grisoni[4], Guillaume De Liège[4], Sandra Nunige[3], Kahina Djaoudi[3], Elvira Pulido-Villena[3], Julie Dinasquet[5,6], Ingrid Obernosterer[6], Philippe Catala[6], Cécile Guieu[1]

[1] Sorbonne Université, CNRS, Laboratoire d'Océanographie de Villefranche, LOV, 06230 Villefranche-sur-Mer, France

[2] CNRS-INSU/IRD/MNHN/UPMC, LOCEAN: Laboratoire d'Océanographie et du Climat: Expérimentation et Approches Numériques, UMR 7159, 75252 Paris Cedex 05, France

[3] Aix-Marseille Université, Université de Toulon, CNRS/INSU, IRD, MIO, UM 110, 13288, Marseille, France

[4] Sorbonne Université, CNRS, Institut de la Mer de Villefranche, IMEV, 06230 Villefranche-sur-Mer, France

[5] Scripps Institution of Oceanography, University of California San Diego, USA

[6] CNRS, Sorbonne Université, Laboratoire d'Océanographie Microbienne, LOMIC, F-66650 Banyuls-sur-Mer, France

Correspondence to: Frédéric Gazeau (f.gazeau@obs-vlfr.fr)

Keywords: Mediterranean Sea; Atmospheric deposition; Plankton community; Ocean acidification; Ocean warming

Abstract

In Low Nutrient Low Chlorophyll areas, such as the Mediterranean Sea, atmospheric fluxes represent a considerable external source of nutrients likely supporting primary production especially during periods of stratification. These areas are expected to expand in the future due to lower nutrient supply from sub-surface waters caused by climate-driven enhanced stratification, likely further increasing the role of atmospheric deposition as a source of new nutrients to surface waters. Whether plankton communities will react differently to dust deposition in a warmer and acidified environment remains, however, an open question. The potential impact of dust deposition both in present and future climate conditions was investigated in three perturbation experiments in the open Mediterranean Sea. Climate reactors (300 L) were filled with surface water collected in the Tyrrhenian Sea, Ionian Sea and in the Algerian basin during a cruise conducted in the frame of the PEACETIME project in May/June 2017. The experiments comprised two unmodified control tanks, two tanks enriched with a Saharan dust analog and two tanks enriched with the dust analog and maintained under warmer (+3 ºC) and acidified (-0.3 pH unit) conditions. Samples for the analysis of an extensive number of biogeochemical parameters and processes were taken over the duration (3-4 d) of the experiments. Dust addition led to a rapid release of nitrate and phosphate, however, nitrate inputs were much higher than phosphate. Our results showed that the impacts of Saharan dust deposition in three different basins of the open Northwestern Mediterranean Sea are at least as strong as those observed previously, all performed in coastal waters. The effects of dust deposition on biological stocks were different for the three investigated stations and could not be attributed to differences in their degree of oligotrophy but rather to the initial metabolic state of the community. Ocean acidification and warming did not drastically modify the composition of the autotrophic assemblage with all groups positively impacted by warming and acidification. Although autotrophic biomass was more positively impacted than heterotrophic biomass under future environmental conditions, a

stronger impact of warming and acidification on mineralization processes suggests a decreased capacity of Mediterranean surface plankton communities to sequester atmospheric CO_2 following the deposition of atmospheric particles.

1. Introduction

Atmospheric deposition is well recognized as a significant source of micro- and macro-nutrients for surface waters of the global ocean (Duce et al., 1991; Jickells et al., 2005; Moore et al., 2013). The potential modulation of the biological carbon pump efficiency and the associated export of carbon by atmospheric deposition events are still poorly understood and quantified (Law et al., 2013). This is especially true for Low Nutrient Low Chlorophyll (LNLC) areas where atmospheric fluxes can play a considerable role in nutrient cycling and that represent 60% of the global ocean surface area (Longhurst et al., 1995) as well as 50% of global carbon export (Emerson et al., 1997). These regions are characterized by low availability of macronutrients (N, P) and/or micronutrients (trace metals, in particular Fe) that can severely limit or co-limit phytoplankton growth during large periods of year.

The Mediterranean Sea is a typical example of these LNLC regions with overall surface chlorophyll *a* concentrations below 0.2 μg L^{-1} all year round, except in the Ligurian Sea where relatively large blooms can be observed in late winter-early spring (Mayot et al., 2016). Recent estimates indicate that the atmospheric input of nutrients in the Mediterranean Sea is within the same order of magnitude as riverine inputs (Powley et al., 2017), and, therefore, a considerable external source of nutrients (Richon et al., 2018). Atmospheric deposition originates both from natural (mainly Saharan dust) and anthropogenic sources (e.g. Bergametti et al., 1989; Desboeufs et al., 2018). Dust deposition, mostly in the form of pulsed inputs, is mainly associated with wet deposition (Loÿe-Pilot and Martin, 1996). Ternon et al. (2010) reported an average annual dust flux over four years of 11.4 g m^{-2} yr^{-1} (average during the period 2003–2007) at the DYFAMED station in the Northwestern Mediterranean Sea. In this region, the most important events reported in the 2010 decade amounted to ~22 g m^{-2} (Bonnet and Guieu, 2006; Guieu et al., 2010b).

Atmospheric deposition provides new nutrients to surface waters (Guieu et al., 2010b; Kouvarakis et al., 2001; Markaki et al., 2003; Ridame and Guieu, 2002), Fe (Bonnet and Guieu, 2006) and other trace metals(Desboeufs et al., 2018; Guieu et al., 2010b; Theodosi et al., 2010), representing significant inputs likely supporting primary production in particular during the period of stratification in spring/summer (Bonnet et al., 2005; Ridame and Guieu, 2002), although no direct correlation between dust and ocean color could be found from long series of satellite observation in that part of the Mediterranean basin (Guieu and Ridame, 2020).

Previous micro- and mesocosm experiments have shown that wet dust deposition events in the Northwestern Mediterranean Sea (the dominant deposition mode in that basin) are a stronger source of bioavailable nutrients compared to dry deposition. Wet deposition provides both new N and P while dry deposition supplies primarily P and, in contrast to wet deposition, does not stimulate the growth of the autotrophic community with the exception of diazotrophs (Ridame et al., 2013), resulting in no significant increase in chlorophyll *a* concentrations and primary production (Guieu et al., 2014a). In addition, wet dust deposition also modifies the bacterial assemblage leading to even stronger enhancements of heterotrophic production and respiration rates (Pulido-Villena et al., 2014). The carbon budget established from four artificial seeding experiments during the DUNE project (Guieu et al., 2014a) showed that by stimulating predominantly heterotrophic bacteria, atmospheric wet dust deposition can enhance the heterotrophic behavior of these oligotrophic waters. This has the potential to reduce organic carbon export to deep waters during the winter mixing period (Pulido-Villena et al., 2008) and ultimately limit net atmospheric CO_2 drawdown.

Conversely, the deposition of lithogenic particle from Saharan dust can promote aggregation and ballast organic matter leading to enhanced vertical export of organic carbon (Bressac et al., 2014; Desboeufs et al., 2014; Louis et al., 2017a; Ternon et al., 2010). These lithogenic processes can represent a major part of the carbon export following a dust deposition

98 event (up to 50% during the DUNE experiment; Bressac et al., 2014). Recently, Louis et al.
99 (2017a) showed that Saharan dust deposition can also trigger the abiotic formation of transparent
100 exopolymeric particles (TEP), leading to the formation of organic-mineral aggregates, a
101 formation process that is highly dependent on the quality and quantity of TEP-precursors initially
102 present in seawater.

103 In response to ocean warming and increased stratification, nutrient cycling in the open
104 ocean is being and will continue to be perturbed in the next decades with regionally variable
105 impacts (IPCC, 2019). Overall, LNLC areas are expected to expand in the future (Irwin and
106 Oliver, 2009; Polovina et al., 2008) due to thermal stratification related reduction of nutrients
107 supply from sub-surface waters (Behrenfeld et al., 2006). As such, the role of atmospheric
108 deposition as a source of new nutrients to surface waters might increase. Ongoing warming and
109 acidification (IPCC, 2019) are also evidenced in the Mediterranean Sea (e.g. Kapsenberg et al.,
110 2017; The Mermex group, 2011). Whether or not plankton communities will respond differently
111 to dust deposition in future conditions is still largely unknown. Although dependent on resource
112 availability, it is well known that remineralisation by bacteria is subject to positive temperature
113 control (López-Urrutia and Morán, 2007). Given that warming has no effect on primary
114 productivity when plankton communities are nutrient limted (Marañón et al., 2018), temperature
115 increase will most likely further push the balance towards net heterotrophy in oligotrophic areas.

116 In contrast, an *in situ* mesocosm experiment conducted during the summer stratification
117 period in the Northwestern Mediterranean Sea showed that the plankton community was not
118 sensitive to ocean acidification under strong nutrient limitation (Maugendre et al., 2017, and
119 references therein). A batch experiment (Maugendre et al., 2015) showed that, under nutrient-
120 depleted conditions in late winter, ocean acidification has a very limited impact on the plankton
121 community and that small species (e.g. Cyanobacteria) might benefit from warming with a
122 potential decrease of the export and energy transfer to higher trophic levels. In contrast, in more

eutrophic (coastal) conditions, Sala et al. (2016) showed that ocean acidification had a positive effect on phytoplankton, especially on the pico and nano size classes. Similarly, Neale et al. (2014) showed that ocean acidification could lead to enhanced chlorophyll levels under low light conditions with an opposite effect under high irradiance, in coastal communities of the Alboran Sea.

To date and to the best of our knowledge, there have been no attempts to evaluate the behavior of plankton communities influenced by atmospheric deposition in the context of future temperature and pH changes. Such experiments were, therefore, conducted in the framework of the PEACETIME project (ProcEss studies at the Air-sEa Interface after dust deposition in the MEditerranean sea; http://peacetime-project.org/) on board the R/V "Pourquoi Pas?" during May/June 2017. The project aimed at studying and parameterizing the chain of processes occurring in the Mediterranean Sea driven by atmospheric deposition events including under on-going environmental changes (Guieu et al., 2020). During the cruise, three perturbation experiments were conducted in climate reactors (300 L tanks) filled with surface water collected in the Tyrrhenian Sea (TYR), Ionian Sea (ION) and Algerian basin (FAST; Fig. 1). Six tanks were used to follow simultaneously and with a high temporal resolution, the evolution of biological activity and stocks, nutrients, dissolved organic matter as well as particles dynamics and export, following a dust deposition event simulated, both under present environmental conditions and under a realistic climate change scenario for 2100 (ca. +3 °C and -0.3 pH units; IPCC, 2013). In this manuscript, we will present the general setup of the experiments and the evolution of nutrient and plankton communities (heterotrophic and autotrophic prokaryotes, photosynthetic eukaryotes as well as micro- and meso-zooplankton). Other manuscripts, related to these experiments in this special issue, focus on plankton metabolism (primary production, heterotrophic prokaryote production) and carbon export (Gazeau et al., 2021), microbial food

147 web (Dinasquet et al., 2021), nitrogen fixation (Céline Ridame, unpublished results) and on the
148 release of insoluble elements (Fe, Al, REE, Th, Pa) from dust (Roy-Barman et al., 2021).

2. Material and Methods

2.1. General setup

Six experimental tanks (300 L; Fig. 2), in which the irradiance spectrum and intensity can be finely controlled and future ocean acidification and warming conditions can be fully reproduced, were installed in a temperature-controlled container. The tanks are made of trace-metal free high-density polyethylene (HDPE) with a height of 1.09 m, a diameter of 0.68 m, a surface area of 0.36 m^2 and a volume of 0.28 m^3. Each tank was equipped with a lid containing six rows of LEDs (Alpheus©). Each of these rows were composed of blue, green, cyan and white units in order to mimic the natural sun spectrum. At the conical base of each tank, a polyethylene (PE) bottle was screwed onto a polyvinyl chloride (PVC) valve that remained open during the duration of the whole experiment to collect the sinking material. Photosynthetically active radiation (PAR; 400-700 nm) and temperature were continuously monitored in each tank using respectively QSL-2100 Scalar PAR Irradiance Sensors (Biospherical Instruments©) and pt1000 temperature sensors (Metrohm©) connected to a D230 datalogger (Consort©).

Prior to the start of the experiments, tanks were cleaned following the protocol described by Bressac and Guieu (2013). Three sets of experiments were carried out at the long duration stations ION, TYR and FAST, respectively, and comprised two unmodified control tanks (C1 and C2), two tanks enriched with Saharan dust (D1 and D2) and two tanks enriched with Saharan dust and maintained under warmer (+3 ºC) and acidified (-0.3 pH unit) conditions (G1 and G2). The atmosphere above tanks C1, C2, D1 and D2 was flushed with ambient air (ca. 400 ppm, 6 L min^{-1}) and tanks G1 and G2 were flushed with air enriched with CO_2 (ca. 1000 ppm, 6 L min^{-1}) in order to prevent CO_2 degassing from the acidified tanks. CO_2 partial pressure (pCO_2) in both ambient air and CO_2-enriched air was monitored using two gas analysers (LI-820, LICOR©).

172 The CO_2 concentration in the CO_2-enriched air was manually controlled through small injections
173 of pure CO_2 (Air Liquide©) using a mass flow controller. Mixing in the tanks was ensured by a
174 rotative PVC blade (9 rpm) mimicking natural turbulence

175 The tanks were filled by means of a peristaltic pump (Verder© VF40 with EPDM hose,
176 flow of 1200 L h^{-1}) collecting seawater below the base of the boat at around 5 m, used to supply
177 continuously surface seawater to a series of instruments during the entire campaign. In order to
178 homogeneously fill the tanks, the flow was divided into six HDPE pipes distributing the water
179 simultaneously into the different tanks. The procedure was started at the end of the day at all
180 three stations and took approximately 2 h (including rinsing and initial sampling. While filling
181 the tanks, samples were taken for the measurements of selected parameters (sampling time = t-
182 12h before dust seeding; Table 1). After filling the tanks, seawater in tanks G1 and G2 was
183 slowly warmed overnight using 500 W heaters, controlled by temperature-regulation units
184 (COREMA©), to reach an offset of +3 °C. ^{13}C-bicarbonate was added to all tanks at 4:00 am
185 (local time; Gazeau et al., 2021) and at 4:30 am G1 and G2 were acidified by addition of CO_2-
186 saturated filtered (0.2 µm) seawater (~1.5 L in 300 L; collected when filling the tanks at each
187 station) to reach a pH offset of -0.3. Further samples for a range of parameters were taken
188 (sampling time = t0, Table 1), followed by dust seeding carried out between 7:00 and 9:00 (local
189 time) in tanks D1, D2, G1 and G2. The same dust analog flux was applied as in the DUNE 2009
190 experiments described in Desboeufs et al. (2014). The dust was derived from the <20 µm
191 fraction of soil collected in Southern Tunisia (a major source for material transported and
192 deposited in the Northwestern Mediterranean) consisting of quartz (40%), calcite (30%) and clay
193 (25%) with most particles (99%) smaller than 0.1 µm (Desboeufs et al., 2014). The collected
194 material underwent an artificial chemical aging process by addition of nitric and sulfuric acid
195 (HNO_3 and H_2SO_4, respectively) to mimic cloud processes during atmospheric transport of
196 aerosol with anthropogenic acid gases (Guieu et al., 2010a, and references therein). To mimic a

realistic wet flux event for the Mediterranean of 10 g m^{-2}, 3.6 g of this analog dust were quickly diluted in 2 L ultrahigh-purity water (UHP water; 18.2 MΩ cm^{-1} resistivity), and sprayed at the surface of the tanks using an all-plastic garden sprayer (duration = 30 min). The total N and P mass in the dust were 1.36 ± 0.09% and 0.055 ± 0.003%, respectively (see Desboeufs et al., 2014, for a full description of dust chemical composition). Biogeochemical parameters and processes measured during the experiments are listed in Table 1. The experiment lasted 3 days (72 h) at stations TYR and ION and 4 days (96 h) at station FAST, as constrained by the time available between stations. Seawater sampling was conducted 1 h (t1h), 6 h (t6h), 12 h (t12h), 24 h (t24h), 48 h (t48h) and 72 h (t72h) after dust additions in all three experiments with an additional sample after 96 h (t96h) at FAST). Acid-washed silicone tubes were used for transferring the water collected by gravity from the tanks to the different vials or containers.

2.2. Analytical methods

2.2.1. Carbonate chemistry

Seawater samples for pH measurements were stored in 300 mL glass bottles with a glass stopper, pending analysis on board (within 2 h). Samples were transferred to 30 mL quartz cells and absorbances at 434, 578 and 730 nm were measured at 25 °C on an Cary60 UV-Spectrophotometer (Agilent©) before and after addition of 50 µL of purified meta-cresol purple provided by Robert H. Byrne (University of South Florida, USA) following the method described by Dickson et al. (2007). pH on the total scale (pH_T) was computed using the formula and constants of Liu et al. (2011). The accuracy of pH measurements (0.007 pH units) was estimated using a TRIS buffer solution (salinity 35, provided by Andrew Dickson, Scripps university, USA).

Seawater samples (500 mL) for total alkalinity (A_T) measurements were filtered on GF/F membranes and analyzed onboard within one day. A_T was determined potentiometrically using a Metrohm© titrator (Titrando 888) and a glass electrode (Metrohm©, ecotrode plus) calibrated using first NBS buffers (pH 4.0 and pH 7.0, to check that the slope was Nernstian) and then using a TRIS buffer solution (salinity 35, provided by Andrew Dickson, Scripps university, USA). Triplicate titrations were performed on 50 mL sub-samples at 25 ºC and A_T was calculated as described by Dickson et al. (2007). Titrations of standard seawater provided by Andrew Dickson (Scripps university, USA; batch 151) yielded A_T values within 5 µmol kg^{-1} of the nominal value and a standard deviation of 1.5 µmol kg^{-1} (n = 40).

All parameters of the carbonate chemistry were determined from pH_T, A_T, temperature, salinity, as well as phosphate and silicate concentrations using the R package seacarb. Propagation of errors on computed parameters was performed using the new function "error" of this package, encompassing errors associated with the estimation of A_T, pH_T as well as errors on the dissociation constants (Orr et al., 2018).

2.2.2. Nutrients

Seawater samples for dissolved nutrients were collected in polyethylene bottles after passage through sterile membrane filter capsules (Sartobran″ 300; 0.2 µm) connected to the sampling tubes of each tank (Sartobran© 300; 0.2 µm), and analyzed directly on board. Nitrate + nitrite (NO_x) and silicate ($Si(OH)_4$) measurements were conducted using a segmented flow analyzer (AAIII HR Seal Analytical©) according to Aminot and Kérouel (2007) with a detection limit of 0.05 µmol L^{-1} for NO_x and 0.08 µmol L^{-1} for $Si(OH)_4$. In addition, at t-12h, NO_x was also analysed by spectrometry at 540 nm, with a 1 m Liquid Waveguide Capillary Cell (LWCC), with a detection limit of ~10 nmol L^{-1} and the reproducibility was ~6%. Ammonium concentrations in samples from t-12h were also measured on board using a Fluorimeter TD-700

(Turner Designs©) according to Holmes et al. (1999). This later method is based on the reaction of ammonia with orthophtaldialdehyde and sulfite and has a detection limit of 0.01 µmol L^{-1}. Dissolved inorganic phosphorus (DIP) concentrations were quantified using the Liquid Waveguide Capillary Cell (LWCC) method according to Pulido-Villena et al. (2010). The LWCC was 2.5 m long and the detection limit was 1 nmol L^{-1}.

2.2.3. Pigments

For pigment analysis, 2.5 L seawater from the tanks were filtered onto GF/F filters, immediately frozen in liquid nitrogen and stored at -80 ºC pending analysis at the SAPIGH analytical platform at the Institut de la Mer de Villefranche (IMEV, France). Filters were sonicated at -20 ºC in 3 mL methanol (100%) containing an internal standard (vitamin E acetate, Sigma©) and clarified one hour later by vacuum filtration through GF/F filters. The extracts were rapidly analyzed (within 24 h) on a complete Agilent© Technologies 1200 series HPLC system. The pigments were separated and quantified as described in Ras et al. (2008).

2.2.4. Flow cytometry

For flow cytometry, samples (4.5 mL) were fixed with glutaraldehyde grade I (1% final concentration), and incubated for 30 min at 4 °C, quick-frozen in liquid nitrogen and stored at -80 °C until analysis. Samples were thawed at room temperature. Counts were performed on a FACSCanto II flow cytometer (Becton Dickinson©) equipped with 3 air-cooled lasers: blue (argon 488 nm), red (633 nm) and violet (407 nm). Following Marie et al. (2010), *Synechococcus* spp. was discriminated by its strong orange fluorescence (585 ± 21 nm), and autotrophic pico- and nano-eukaryotes were discriminated by their scatter signals of red fluorescence (> 670 nm). For the enumeration of heterotrophic prokaryotes, cells were stained with SYBR Green I (Invitrogen – Molecular Probes) at 0.025% (vol / vol) final concentration for

15 min at room temperature in the dark. Stained prokaryotic cells were discriminated and enumerated according to their right-angle light scatter (SSC) and green fluorescence at 530/30 nm. Heterotrophic prokaryotes were distinguished from autotrophic prokaryotes based on the green vs. red fluorescent signal. The same procedure was used for the enumeration of HNF, after staining with 0.05% (v/v) final SYBR Green I concentration for 15-30 min at room temperature in the dark (Christaki et al., 2011). Fluorescent beads (1.002 µm; Polysciences Europe©) were systematically added to all samples as internal standard. Cell concentrations were determined based on counts and flow rate, estimated with TruCount beads (BD biosciences©). Biomass of each group were estimated based on conversion equations and/or factors found in the literature (see section 2.3.2).

2.2.5. Micro-phytoplankton and -heterotrophs

At t-12h, 500 mL samples were collected in glass vials and immediately preserved with 5% final concentration acidic Lugol's solution. Back at the Laboratoire d'Océanographie de Villefranche (LOV, France), 100 mL aliquots were transferred to sedimentation chambers (Utermohl) and counted under an inverted microscope at x 200 to x 400 magnification.

2.2.6. Mesozooplankton

At the end of each experiment, the sedimentation bottles were removed, fixed with formaldehyde 4% (see Gazeau et al., 2021) and stored for analysis back in the home laboratory. Subsequently, the valve at the base of each tank, that allowed retrieval of the sedimentation bottles without disturbance, was opened, the remaining water inside the tanks (165-180 L at TYR; 172.5 L at ION and 150 L at FAST) as filtered through a 100 µm mesh size PVC sieve. The organisms retained were gently removed using a washing bottle filled with filtered seawater (0.2 µm), and transferred directly in a 250 mL bottle and fixed with 4% final concentration

formaldehyde. These samples were processed using a ZooSCAN (Hydroptic©; Gorsky et al., 2010) at the PIQv-platform of EMBRC-France. Organisms were identified and counted using automatic classification with a reference dataset in EcoTaxa (https://ecotaxa.obs-vlfr.fr/, last access: 17/04/2020), followed by manual validation.

2.3. Data analyses

2.3.1. Nutrient inputs from dust

The maximum percentage of dust-born dissolved N and P was estimated based on initial N and P composition of the dust analog (see section 2.1; Desboeufs et al., 2014) and maximal concentrations observed in tanks D and G at t1h and t6h after seeding, as follows:

$$\%_{dissolution} = \frac{CONC_{max} - CONC_{init}}{CONC_{dust}} . 100 \quad (1)$$

where $CONC_{init}$ is the concentration of the corresponding nutrient in each tank before seeding (t0), $CONC_{max}$ corresponds to the concentration of the corresponding nutrient in each tank when nutrient concentration was at a maximum within the first 6 h after seeding, and $CONC_{dust}$ is the maximum potential concentration, assuming a 100% dissolution from dust analog (based on dust content; Desboeufs et al. 2014; section 2.1).

2.3.2. Autotrophic and heterotrophic biomass

Given that samples for micro-phytoplankton counts were taken only at t-12h, as a first approximation, autotrophic biomass was estimated as the sum of *Synechococcus*, autotrophic pico-eukaryotes and nano-eukaryotes biomass (based on flow cytometry). Conversion of abundances to to carbon units was carried out assuming 250 fg C $cell^{-1}$ *for Synechococcus* (Kana and Glibert, 1987). The biovolume to carbon content relationship of Verity et al. (1992) was used

310 for autotrophic pico- and nano-eukaryotes assuming a spherical shape and a diameter of 2 and 6
311 μm, respectively. Heterotrophic biomass was computed as the sum of heterotrophic prokaryotes
312 (HP) biomass and heterotrophic nanoflagellates (HNF) biomass. Conversion to carbon biomass
313 were done assuming 20 fg C $cell^{-1}$ (Lee and Fuhrman, 1987) for heterotrophic prokaryotes and
314 220 fg C μm^{-3} (Børsheim and Bratbak, 1987) with a spherical shape and 3 μm diameter for
315 heterotrophic nanoflagellates. The ratio of autotrophic and heterotrophic biomass during the
316 experiments was used to evaluate the trophic status of the investigated communities and its
317 evolution. Finally, a proxy for micro-phytoplankton biomass (B_{micro}) was estimated following
318 Vidussi et al. (2001), as the sum of Fucoxanthin and Peridinin.

3. Results

3.1. Initial conditions

Initial conditions at the three sampling stations while filling the tanks (t-12h before seeding) are shown in Table 2. pH_T, total alkalinity concentrations increased from west to east (Table 2). NO_x and DIP concentrations followed different patterns with highest NO_x values at station FAST and highest DIP concentrations at station TYR. Consequently, the lowest NO_x:DIP ratio was measured at TYR (0.8), compared to ION and FAST (2.8 and 4.6, respectively). Ammonium concentrations ranged between 0.045 μmol L^{-1} to below detection limit at FAST. Silicate concentrations were similar at stations TYR and ION (~ 1 μmol L^{-1}) and higher than at station FAST (0.64 μmol L^{-1}).

Very low chlorophyll *a* concentrations were measured at the three stations (0.063 - 0.072 μg L^{-1}). The proportion of the different major pigments (Fig. 3) indicates that phytoplankton communities were similar with a dominance of Prymnesiophytes (i.e. 19'-hexanoyloxyfucoxanthin; Ras et al., 2008) followed by Cyanobacteria (i.e. Zeaxanthin; Ras et al., 2008) at stations TYR and ION. In contrast, at station FAST, the plankton community was clearly dominated by photosynthetic prokaryotes (i.e. Zeaxanthin and Divinyl-chlorophyll *a* as proxies for Cyanobacteria and Prochlorophytes, respectively; Ras et al., 2008). At all three stations, the proportion of pigments representative of larger species (i.e. Fucoxanthin and Peridinin; diatoms and dinoflagellates respectively; Ras et al., 2008) were very small (< 5%).

At all stations, autotrophic nanoplankton contributed most to total biomass. Autotrophic and heterotrophic biomass and abundances were highest at station FAST, followed by ION for the autotrophs and TYR for heterotrophs (Table 2). Differences in standing stocks between stations where more pronounced for the heterotrophs. As a consequence, the ratio between

autotrophic biomass and heterotrophic biomass ranged from ~0.6 at TYR and FAST to 1.3 at ION.

3.2. Conditions of irradiance, temperature and pH during the experiments

Irradiance levels during the experiments are shown in Fig. 4. Decrease in water transparency after dust addition was observed at all three stations with the lowest impact at station FAST where irradiance levels decreased by only 60 μmol photons m^{-2} s^{-1} after dust addition, reaching similar levels as observed for tanks D and G. At station TYR, a more pronounced decrease was observed in acidified and warmed tanks (G1 and G2) with a decrease of daily average maximum irradiance of ~ 60 and ~ 160 μmol photons m^{-2} s^{-1} compared to dust-amended tanks D and controls, respectively. Temperature control (Fig. 4) was not optimal showing deviations between replicates of treatment G of up to 1.0 °C (station FAST). Temperature in controls and D tanks displayed a daily cycle, increasing during the day and decreasing at night (Fig. 4). The differences between the warmed treatment (G) and the other tanks were +3, +3.2 and +3.6 °C at TYR, ION and FAST, respectively.

Addition of CO_2-saturated filtered seawater led to a decrease in pH_T from 8.05 ± 0.004 (average ± SD of C1, C2, D1 and D2 at t0) to 7.74 (average between G1 and G2) at station TYR, from 8.07 ± 0.002 to 7.78 at station ION and from 8.05 ± 0.001 to 7.72 at station FAST (Fig. 5). pH_T levels remained more or less constant in the control and D tanks during all three experiments with no clear impact of dust addition. In G tanks, pH levels gradually increased during the experiments with larger variability between duplicates. These increases remained moderate thanks to the flushing of CO_2-enriched air above the tanks (pCO_2 of 1017 ± 11, 983 ± 96, 1023 ± 25 ppm at TYR, ION and FAST, respectively; data not shown). Partial pressure of CO_2 in ambient air was 410 ppm, similar for the three stations. In all experiments, the addition of

^{13}C-bicarbonate led to an increase of total alkalinity between 6 and 11 μmol kg^{-1} at t0. Dust addition, right after t0 in tanks D and G, led to a A_T decrease between 8 and 16 μmol kg^{-1} at t24h with no apparent effects of warming and acidification. Overall, no large changes in A_T were observed during the experiments (Fig. 5).

3.3. Changes in nutrient concentrations

Dust addition led to a rapid increase in NO_x (~ 11 μmol L^{-1} as observed during the first 6 h; Fig. 6; Table 3) at all three stations with no differences between treatments D and G. The corresponding percent dissolution of N from dust ranged between 94 and 99%. In contrast, maximum DIP release was much smaller, ranging between 20 and 37 nmol L^{-1}, with slightly higher values at FAST (31-37 nmol L^{-1}) as compared to the other stations. Percent dissolution for DIP corresponded to 9.2 to 17.3% of total phosphorus contained in dust. As a consequence, NO_x:DIP ratios increased from initial values below 5 to above 300, within 6 h after dust seeding, in tanks D and G (Fig. 6).

After the rapid increase of N and P, both nutrients decreased with time. While nutrient variability was small in control tanks (NO_x and DIP variations below 20 and 3 nmol L^{-1}, respectively), large decrease in both elements occured in dust amended tanks (D and G; Table 4). Similar linear decrease in NO_x were observed throughout the experiments at stations TYR and ION with no visible differences between tanks D and G. In contrast, at station FAST, a more pronounced decrease in NO_x was observed in dust-amended (D and G) tanks, as well as in warmed and acidified tanks relative to the D treatment. Nevertheless, at all stations, NO_x concentrations in D and G treatments remained far above ambient levels throughout the experiments (> 9 μmol L^{-1}). Abrupt decreases in DIP were observed during the three experiments after the initial increase. At station TYR, after 24 h, all DIP released from dust decreased to initial levels in tanks G while it took two more days to reach initial levels in tanks D. In contrast,

at station ION, no clear difference in DIP dynamics was observed between treatments D and G, with concentrations that decreased rapidly during the first 24 h but remained above initial levels until the end of the experiment. At station FAST, similarly to station TYR, DIP decreased rapidly from t12h in treatment G, reaching levels close to initial conditions at the end of the experiment. DIP decrease was much lower in treatment D (Table 4) with concentrations maintained far above ambient levels throughout the experiment. As a consequence of the differences between NO_x and DIP dynamics as well as differences among stations, NO_x:DIP ratio increased, with clear differences between stations (Fig. 6), and remained much higher than in the controls.

At all stations, silicate concentrations were higher in dust amended tanks relative to the controls. At TYR, while concentrations remained stable in control tanks, they increased linearly with time in the other tanks (D and G) with no apparent effect of the imposed increase in temperature and decrease in pH (i.e. tanks G). Difference in $Si(OH)_4$ concentrations between dust amended treatments (D and G) and controls was ~0.1 μmol L^{-1} at the end of the experiment. At station ION, after an initial decrease in concentrations between t-12h and t0, concentrations increased in all tanks until the end of the experiment with higher values in dust amended tanks (D and G) than in controls and no difference between D and G treatments. In contrast, at FAST, concentrations increased from t-12h to t48h (with higher values in dust amended tanks) and decreased onward until the end of the experiment. At the end of the experiment (t96h), $Si(OH)_4$ concentrations were higher in the G treatment than in the D treatment which were similar to the controls.

3.4. Changes in biological stocks

Temporal dynamics in biological parameters showed very different patterns at each station. At TYR, total chlorophyll *a* concentrations did not change in the dust amended D tanks

(Fig. 7) and even led to slightly decreased values 24 h after dust addition (e.g. -35 to -38% in D1 and D2, respectively as compared to controls; Table 5). No clear effects of dust addition (tanks D vs. C) were detectable for all groups based on pigment analyses (Fig. 7). Results obtained based on flow cytometry counts (Fig. 8) were coherent with these observations and showed stronger decreases in cell abundances for < 20 µm autotrophic groups in tanks D1 and D2 (-77 to -80%). In contrast, the abundance of heterotrophic prokaryotes (HP) increased rapidly after dust addition both under ambient (+53-68%) and future (+68%) environmental conditions, with no clear difference among treatments. In warmed and acidified tanks (G), strong discrepancies between the duplicates were observed for pigments and autotrophic cell abundances: tank G1 showed moderate increases for all variables with the exception of autotrophic pico-eukaryotes, while in G2 all variables responded strongly to dust addition with maximum relative changes of > 300%, with the exception of autotrophic nano-eukaryotes. While HNF abundances responded positively to the treatments in D1, D2 and G2, abundances increased sharply in tank G1 towards the end of the experiment.

At ION, clear differences between treatments were observed for almost all pigments and cell abundances (Fig. 7, Fig. 8). With the exception of autotrophic nano-eukaryotes and HNF, all variables (pigments and cell abundances) increased as a response to both dust addition and warmed/acidified conditions (Table 5). The maximum relative changes as compared to controls observed for total chlorophyll *a* were 109-183% and 399-426% in tanks D and G, respectively. The highest stimulation by dust addition was observed for *Synechococcus* with +317-390% and +805-1425% increase in abundances in D and G tanks respectively (Table 5). Autotrophic nano-eukaryotes and HNF abundances did not respond to dust addition under ambient conditions but an increase in abundances occured in treatment G. In contrast to observations at TYR, temperature and pH affected heterotrophic prokaryotes in all dust-amended tanks at station ION with a higher impact of dust addition under future environmental conditions.

At station FAST, all biological stocks increased strongly after dust addition (Fig. 7, Fig. 8 and Table 5). Total chlorophyll *a* increased following exponentially until the end of the experiment with slightly lower values observed under ambient environmental conditions (+237-318% in D tanks and ~ +400% in G tanks). Prymnesiophytes (i.e. 19'-hexanoyloxyfucoxanthin) and diatoms (i.e. Fucoxanthin) appeared as the groups benefiting the most from dust addition with no large impacts of warming/acidification while Pelagophytes (i.e. 19'-butanoyloxyfucoxanthin) and green algae (i.e. Total Chlorophyll *b*) showed a stronger response in treatment G. Finally, although Cyanobacteria (i.e. Zeaxanthin) responded faster to dust addition under future environmental conditions (tanks G), this effect attenuated towards the end of the experiment. In contrast to estimates based on pigments, increases in cell abundances did not generally last until the end of the experiments. While abundances of autotrophic pico-eukaryotes increased until t96h in treatment D, abundances sharply declined between t72h and t96h for this group in treatment G. The same trend was observed for *Synechococcus*, although discrepancies between duplicates in treatment D at t96h did not allow drawing conclusions on the behavior of this group by the end of the experiment. Abundances of autotrophic nano-eukaryotes declined sharply between t72h and t96h under present and future conditions. The decline in HP abundances occured earlier during the experiment with moderate maximum relative differences as compared to controls at t48h. HP abundances declined very sharply between t48h and t96h in treatment G, reaching control levels, while this decline was less sharp under present environmental conditions. Finally, HNF dynamics during this experiment was hard to interpret given the large increase in abundances in only one duplicate of treatment G (t24h) followed by a gradual decline.

Abundances of meso-zooplankton at the end of the experiments showed relatively similar values at stations TYR and ION while much higher levels were observed at station FAST (Fig. 9). As a consequence of large variability between duplicates at stations TYR and ION, no clear

464 effects of treatments were detected. At station FAST, although the sample size was too low to
465 statistically test for differences, higher total abundances of meso-zooplankton species were
466 observed in the dust-amended tanks with no differences between ambient and future conditions
467 of temperature and pH. However, differences in abundance were visible between these two
468 treatments for specific groups, with respectively higher abundance of Harosa and lower
469 abundance of Crustacea (other than copepods) and Mollusca in warmed and acidified tanks.

4. Discussion

4.1. Initial conditions

During this study, the mixed layer depth (MLD) was somewhat shallower at TYR (20 m) than at ION and FAST (~ 10 and ~15 m, respectively) at the time of the sampling (Van Wambeke et al., 2020a). Such shallow MLDs are characteristic of the stratified and oligotrophic conditions encountered in the western Mediterranean basin in late spring/early summer (D'Ortenzio et al., 2005). Although direct measurements of NO_x and DIP concentrations using nanomolar techniques (as performed in our study) are scarce in the Mediterranean Sea, the low levels measured during the cruise are in agreement with DIP values reported for the three basins (Djaoudi et al., 2018) and with NO_x and DIP concentrations measured in coastal waters of Corsica in late spring/early summer (Louis et al., 2017b; Pulido-Villena et al., 2014; Ridame et al., 2014). NO_x:DIP molar ratios in surface waters were well below the Redfield ratio (16:1) and are also consistent previous studies. The low NO_x:DIP ratios and nutrient concentrations suggest that communities found at the three stations experienced N and P co-limitation at the start of the experiments, as previously shown by Tanaka et al. (2011). Nutrient enrichment experiments confirmed that, at the three sites, heterotrophic bacteria were mainly N-P co-limited (Van Wambeke et al., 2020b). In contrast to N and P, dissolved Fe in surface seawater, ranged from 1.5 nmol L^{-1} at TYR to 2.5 nmol L^{-1} at ION (Roy-Barman et al., 2021) and were unlikely limiting for biological activity as previously shown in the Mediterranean Sea under stratified conditions (Bonnet et al., 2005; Ridame et al., 2014).

The low total chlorophyll *a* concentrations in surface waters were typical for the Western and Central Mediterranean Sea in late spring/early summer, as estimated from remote sensing (Bosc et al., 2004), and from *in situ* measurements (Manca et al., 2004). While large species (i.e. diatoms, dinoflagellates) represented only ~10% of the total chlorophyll *a* biomass, the

composition of the smaller size phytoplankton communities differed substantially, with autotrophic nano-eukaryotes dominating at stations TYR and ION and a larger contribution from autotrophic pico-eukaryotes and Cyanobacteria at station FAST. Due to their low competitiveness under nutrient limitation, the small contribution of large phytoplankton cells at the start of the experiment is a fingerprint of LNLC areas in general, and of surface Mediterranean waters in late spring and summer (Siokou-Frangou et al., 2010).

Biomass of both heterotrophic nanoflagellates and prokaryotes followed a west to east gradient (FAST > TYR > ION), with high relative contribution by heterotrophs at stations TYR and FAST (60% of biomass) while at ION autotrophs contributed 60% to plankton biomass. Accordingly, net community production (NCP) rates (Gazeau et al., 2021) showed an initial community close to metabolic balance (mean ± SE: -0.06 ± 0.09 μmol O_2 L^{-1} d^{-1}) at ION and highest community respiration rates and consequently lowest NCP rates at station TYR (-1.9 μmol O_2 L^{-1} d^{-1}) suggesting that the autotrophic plankton community was not very active and relied on regenerated nutrients, as shown by the high level of NH_4^+ at the start of the experiment at TYR. In contrast, although slightly heterotrophic (Gazeau et al., 2021) and limited by the low amount of nutrients, the community at FAST showed by the highest levels of ^{14}C production and heterotrophic prokaryote production (Gazeau et al., 2021) as well as N_2 fixation (Céline Ridame, unpublished results). Altogether, the heterotrophic signature of the three investigated stations, although closer to metabolic balance at ION, reflected typical biogeochemical conditions in the Mediterranean Sea during late spring to early summer (Regaudie-de-Gioux et al., 2009).

4.2. Critical assessment of the experimental system and methodology

The experimental tanks used in this study have been successfully validated in previous studies designed to investigate the inputs of macro- and micro-nutrients (e.g. NO_x, DIP, DFe)

518 and the export of organic matter, under close-to-abiotic conditions (natural seawater filtered onto
519 0.2 µm) following simulated wet dust events using the same analog as used in our study (Bressac
520 and Guieu, 2013; Louis et al., 2017a, 2018). Louis et al. (2017a, 2018) further investigated these
521 impacts under lowered pH conditions resulting in a rapid increase of pH levels in the acidified
522 filtered seawater due to CO_2 outgassing (from ~7.4 to ~7.7 in six days). In the present study, our
523 experimental system further allowed to control atmospheric pCO_2 in addition to light and
524 temperature (i.e. climate reactors). Thereby, this allowed to significantly reduce CO_2 outgassing
525 and maintain pH levels close to their targets. The regulation of atmospheric CO_2 was, however,
526 consistently more efficient in tank G2 compared to G1 (Fig. 5), resulting in a small discrepancy
527 in terms of pH (highest difference of 0.04 pH units between the two G tanks at FAST), possibly
528 due to a potential leak or a longer flushing time above tank G1. Nevertheless, as no systematic
529 differences in nutrient dynamics and biological response were observed between the two tanks,
530 these small differences in pH had no detectable effect on the obtained results.

531 The lids above tanks, equipped with LEDs in order to reproduce sunlight intensity and
532 spectrum, were used for the first time during these experiments. While simulated intensities were
533 close to estimates for the Northwestern Mediterranean Sea at 5 m depth in June (~1100 µmol
534 photons m^{-2} s^{-1}; Bernard Gentili, personal communication, 2017) and fairly consistent between
535 duplicates under control and dust-amended conditions, largest differences were also observed
536 between tanks G1 and G2. These discrepancies could result from small differences in PAR
537 sensors calibration and/or of different turbidity related to the amount of particles remaining in the
538 tanks. As for pH, replication in terms of macronutrient dynamics and biological response
539 appeared satisfactory (except at station TYR; see below).

540 Continuous measurements in the tanks showed that temperature was not spatially
541 homogeneous, leading to significant differences among replicates. This was more pronounced
542 for warmed tanks (treatment G) with a maximum average difference over the experimental

543 period of 0.7 °C during the FAST experiment. As for pH and light, these discrepancies did not
544 systematically lead to observable differences in the investigated stocks and processes between
545 duplicates (except at TYR, see below).

546 The necessity to carry out the incubations in a clean container limited our possibility to
547 set up additional replicates for the three treatments. As described above, differences between
548 duplicates were, for the vast majority of studied variables and processes, lower than differences
549 between treatments and appear robust considering the difficulty to incubate plankton
550 communities for which slight differences in initial composition can translate into important
551 differences in dynamics (Eggers et al., 2014). Nevertheless, important discrepancies were
552 detected for autotrophic stocks (in particular Synechococcus) as well as HNF and processes
553 (Gazeau et al., 2021) for the warmed and acidified treatment (tanks G1 and G2) at station TYR.
554 The reasons behind these differences are most likely due to the grazing impact of heterotrophic
555 nano-flagellates on prokaryotic picoplankton (Sherr and Sherr, 1994) in tank G1 where HNF
556 abundance sharply increased during the experiment. Overall, while the methodology used in this
557 study allowed to successfully evaluate the impacts of dust addition under both present and future
558 environmental conditions at two out of three tested waters, the discrepancies at station TYR
559 prevent us from drawing any strong conclusion on the effect of dust addition on the dynamics of
560 the community under future environmental conditions at that station.

561 4.3. Impact of dust addition under present environmental
562 conditions

563 During all experiments, the observed increases in NO_x and DIP few hours after dust
564 addition under present environmental conditions were similar to the enrichment obtained during
565 the DUNE experiments at the surface of the mesocosms (~ 50 m^3) after the simulation of a wet
566 dust deposition using the same dust analog and the same simulated flux (Pulido-Villena et al.,

567 2014; Ridame et al., 2014). The intensity of the simulated wet deposition event (i.e. 10 g m^{-2})
568 represents a high but realistic scenario, as several studies reported even higher short wet
569 deposition events in this area of the Mediterranean Sea (Bonnet and Guieu, 2006; Loÿe-Pilot and
570 Martin, 1996; Ternon et al., 2010). Furthermore, based on previous studies reporting the mixing
571 between dust and polluted air masses during the atmospheric transport of dust particles (e.g.
572 Falkovich et al., 2001; Putaud et al., 2004), we used an evapo-condensed dust analog that mimics
573 the processes taking place in the atmosphere prior to deposition, essentially the adsorption of
574 inorganic and organic soluble species (e.g. sulfate and nitrate; see Guieu et al., 2010a, for further
575 details). The imposed evapo-condensation processes are responsible for the large nitrate
576 releasing capacity of the dust particles used in our study. As a consequence, the addition of new
577 nutrients from dust in our study and during the P and R DUNE experiments were much higher,
578 especially for NO_x, than those observed by Pitta et al. (2017, and references therein) and Ridame
579 et al. (2014) following the simulation of a dry Saharan dust deposition event. This confirms that
580 wet dust deposition is a more efficient source of bioavailable nutrients than dry dust deposition.

581 Although NO_x and DIP increases after dust addition were similar in all experiments, the
582 subsequent dynamics of these elements and the impacts on plankton community composition and
583 functioning were drastically different. While NO_x levels decreased moderately over the course of
584 our experiments due to biological uptake, more abrupt decreases were observed for DIP released
585 by dust, reaching values close to the ones observed in the controls, except at station FAST where
586 concentrations were still above ambient levels at the end of the experiment.

587 Previous experiments on the effect of dust addition in the Mediterranean Sea showed
588 significant increases in chlorophyll *a* concentrations (mean ~90% increase; Guieu and Ridame,
589 2020). Interestingly, no stimulation of autotrophic biomass and primary production rates (Gazeau
590 et al., 2021) was observed in dust-amended tanks under present conditions at station TYR. To the
591 best of our knowledge, this is the first experimental evidence of a complete absence of response

592 from an autotrophic community following dust wet deposition. The absence of response from
593 autotrophic stocks could be due to a tight top-down control by grazers hiding potential responses
594 from the autotrophic community (Lekunberri et al., 2010; Marañón et al., 2010) and/or a
595 competition for nutrients with heterotrophic prokaryotes (Marañón et al., 2010). Feliú et al.
596 (2020) have shown that the mesozooplankton assemblage at TYR was clearly impacted by a dust
597 event that took place nine days before sampling at that station as evidenced from particulate
598 inventory of lithogenic proxies (Al, Fe) in the water column (Bressac et al., 2021), likely
599 stimulating phytoplankton growth and consequently increased the abundance of herbivorous
600 grazers (copepods) and attracted carnivorous species well before the start of the experiment.
601 Heterotrophic bacteria are also limited by inorganic nutrients, mainly DIP, in oligotrophic
602 systems (Obernosterer et al., 2003; Van Wambeke et al., 2001). Recent studies have shown
603 significant increases in heterotrophic bacterial abundance, respiration and/or production
604 following dust deposition (and nutrient enrichment) in these areas (Lekunberri et al., 2010; Pitta
605 et al., 2017; Pulido-Villena et al., 2008; Romero et al., 2011). Heterotrophs appear to be more
606 stimulated by dust pulses than autotrophic plankton with increasing degree of oligotrophy,
607 modulated by the competition for nutrients between phytoplankton and bacteria (Marañón et al.,
608 2010). This response was reflected at station TYR, with heterotrophic prokaryotes reacting
609 quickly and strongly to nutrient addition both in terms of abundances and production rates
610 (Gazeau et al., 2021). These two aforementioned hypotheses are not mutually exclusive, and the
611 quick response of heterotrophic prokaryotes to dust addition is coherent with the net
612 heterotrophy at this station (see 4.1) due to increases in community respiration and decreases in
613 net community production rates in dust-amended as compared to control tanks (Gazeau et al.,
614 2021). Hence, dust addition to surface waters strongly dominated by heterotrophs leads to a
615 reduction of the capacity of these communities to export organic matter and sequester
616 atmospheric CO_2.

In contrast to the dynamics of the experiment at TYR, stimulation of primary producers was observed at stations ION and FAST under present conditions with overall higher impact than previous studies compiled by Guieu and Ridame (2020). The largest increase in chlorophyll *a* concentrations at station FAST is coherent with NO_x decreases observed at this station. Interestingly, at FAST, DIP concentrations were still above ambient conditions at the end of the experiment. Maximum primary production rates (^{14}C-incorporation) at the end of the experiment suggest strong DIP recycling and the dominance of regenerated production towards the end of the experiment (Gazeau et al., 2021). Although, in some cases, *Synechococcus* appeared stimulated by dust addition (Herut et al., 2005; Lagaria et al., 2017; Paytan et al., 2009), Guieu et al. (2014b) showed that, based on the analysis of several aerosols addition studies, this group had generally weak responses to aerosol addition in contrast to nano- and micro-phytoplankton, suggesting that aerosol deposition may lead to an increase in larger phytoplankton. Yet, at stations ION and FAST, the increase in *Synechococcus* abundance in dust-amended tanks was the highest relative to those of pico- and nano-eukaryotes. In particular, at station ION, no clear response to nutrient enrichment was observed for nano-eukaryotes throughout the experiment. However, it must be stressed that our experiments were of a relatively short period (3 to 4 days). The sharp increase in Fucoxanthin paralleled by a decrease in silica, at the end of the experiment at station FAST where DIP limitation was not yet apparent, suggests a delayed response of diatoms as compared to smaller taxa. The sharp decline in nano-eukaryote abundances in dust-amended tanks at the end of the FAST experiment, further suggests that this group reacted quickly to nutrient enrichment and was progressively grazed and/or outcompeted by larger phytoplankton species.

While, all groups of primary producers benefited from nutrient enrichment at FAST, the increases in heterotrophic prokaryote abundances were moderate, leading to an increase of net community production rates throughout the experiment, reaching positive levels and a

642 autotroph:heterotroph ratio of 4, while control tanks remained below metabolic balance (Gazeau
643 et al., 2021). At station ION, the situation was intermediate with a similar enhancement of both
644 autotrophic and heterotrophic stocks and no clear changes in the ratio between autotrophic and
645 heterotrophic biomass (data not shown), although the system evolved towards net autotrophy at
646 the end of the experiment in dust -amended tanks under present environmental conditions
647 (Gazeau et al., 2021).

648 Transfer of newly produced organic matter to higher trophic levels in the different
649 treatments was assessed through the quantification of meso-zooplankton abundance at the end of
650 each experiment. Altogether it is not surprising that an increase in meso-zooplankton abundances
651 was only detected at station FAST where the strongest enhancement of primary production was
652 observed. Such an increase in meso-zooplankton abundance in the dust-amended as compared to
653 control treatment was observed during land-based mesocosm experiments in the Eastern
654 Mediterranean Sea (Pitta et al., 2017).

655 Finally, although no clear effects of dust deposition under present conditions were
656 detectable on autotrophic prokaryotes at station TYR, the strongest increase in N_2 fixation rates
657 was recorded at this station (Céline Ridame, unpublished results). However, the potential impact
658 of this process on NO_x concentration is negligible compared to the very large stock of NO_x
659 present in the dust-amended tanks, as less than 1 nmol L^{-1} d^{-1} of NO_x was produced through N_2
660 fixation (Céline Ridame, unpublished results).

661 4.4. Impact of dust addition under future environmental
662 conditions

663 Few studies have investigated the release and fate of nutrients from atmospheric
664 deposition under climate conditions as expected for the end of the century, and, to the best of our

knowledge, our study represents the first attempt to test for the combined effect of ocean warming and acidification on these processes. The study by Louis et al. (2018), carried out with filtered (0.2 µm mesh size) natural seawater using the same dust analog and flux as in the present study showed that even an extreme ocean acidification scenario (~ -0.6 pH units) does not impact the bioavailability of macro- and micro-nutrients (NO_x, DIP and DFe) in the oligotrophic Northwestern Mediterranean Sea. Similar results were found by Mélançon et al. (2016) in high-nutrient low-chlorophyll (HNLC) waters of the Northeastern Pacific, under a moderate ocean acidification scenario (-0.2 pH units). As no differences were observed for NO_x and DIP concentrations within a few hours following dust addition under present and future environmental conditions, our results agree with these previous findings and further highlights the absence of direct effect of ocean warming (+3 °C) on the release of nutrients from atmospheric particles.

In contrast, different nutrient consumption dynamics were observed between ambient and warmed/acidified tanks. No impacts of warming and acidification could be observed for NO_x at stations TYR and ION due to low net uptake rates compared to the large increase following dust addition. In contrast, at the most productive station FAST, as a consequence of strongly enhanced biological stocks (see thereafter) and metabolic rates (Gazeau et al., 2021), larger NO_x consumption rates were shown under future environmental conditions.

The differences in DIP dynamics between the two dust-amended treatments were more complex to interpret. A clear feature of our experiments is that, in contrast to present day pH and temperature conditions, all the stock of DIP released from dust was consumed at the end of the three experiments under future conditions. The rate of decrease differed depending on the station. While DIP dynamics were quite similar between tanks maintained under present and future environmental conditions at ION, warming and acidification induced a faster decrease of DIP at TYR and FAST, with a full consumption of the released DIP within 24 h. An interesting

690 outcome at station TYR was that, despite the important discrepancies observed for autotrophic
691 stocks and metabolic rates between the duplicates G1 and G2 (see section 4.2), a similar
692 dynamics was observed for DIP concentrations in these tanks. As heterotrophic prokaryote
693 biomass and production rates (Gazeau et al., 2021) did not differ between these duplicate tanks,
694 this further highlights the clear dominance of heterotrophic processes at this station, a dominance
695 which was exacerbated by dust addition under future environmental conditions, leading to an
696 even stronger heterotrophic state at the end of this experiment (Gazeau et al., 2021).

697 At station ION, large impacts of warming and acidification were found with twice the
698 chlorophyll *a* concentrations than in the dust amended D tanks. At this station, all autotrophic
699 groups increased with ocean acidification and warming. *Synechococcus* and to a lesser extent
700 pico-eukaryotes showed the strongest response. Yet these differences in abundance did not lead
701 to detectable changes in the composition of the autotrophic assemblage, with nano-eukaryote
702 largely dominating carbon biomass at the end of this experiment (62% in treatment G vs. 64% in
703 treatment D). Although the ratio between autotrophic and heterotrophic biomass appeared
704 positively impacted under future environmental conditions, reaching values of up to 2 at the end
705 of the experiment, warming and acidification led to a decrease in net community production
706 (Gazeau et al., 2021) suggesting that in the coming decades the capacity of surface seawater to
707 sequester anthropogenic CO_2 will be lowered.

708 Similarly, at FAST, all phytoplankton groups were impacted positively by warming and
709 acidification with the strongest changes detected for *Synechococcus* as compared to present
710 environmental conditions. However, in contrast to station ION, all groups reached maximal
711 abundances (and carbon biomass) after 3 days of incubations, thereafter drastically decreasing
712 most likely as a consequence of DIP limitation (see above). It must be stressed that this pattern
713 could not be observed from pigments as no samples were taken for these analyses after 3 days of
714 incubation. Also, in contrast to station ION, the abundance of heterotrophic prokaryotes in the

715 warmer and acidified treatment reached a maximum after 2 days of incubations and then
716 decreased rapidly to reach levels observed in the control treatment. This suggests that
717 heterotrophic prokaryotes were the first to suffer from DIP limitation and further highlights the
718 dominance of autotrophs in terms of nutrient consumption at this station. Although the ratio
719 between autotrophic and heterotrophic biomass increased under future environmental conditions
720 at ION, Gazeau et al. (2021) reported on a decrease in net community production rates in this
721 treatment as compared to ambient environmental conditions, suggesting that, in the future,
722 nutrient release from dust will lead to a lesser sequestration capacity of surface waters for
723 atmospheric CO_2.

724 The positive effects of warming and acidification on the abundance of mostly small (< 20
725 μm) phytoplankton taxa, as observed at ION and FAST, are in line with previously published
726 studies. Although the effect of ocean acidification on small autotrophic species shows a wide
727 range (e.g. Dutkiewicz et al., 2015), there is increasing evidence that small phytoplankton
728 species will be favored in a warmer ocean (e.g. Chen et al., 2014; Daufresne et al., 2009; Morán
729 et al., 2010). Our experimental protocol was not conceived to discriminate temperature from pH
730 effects, however results concur with those of Maugendre et al. (2015) which further suggested
731 temperature over elevated CO_2 as the main driver of increased picophytoplankton abundance in
732 the Mediterranean Sea.

733 These enhanced fertilizing effects on primary producers at ION and FAST, under future
734 as compared to present environmental conditions, did not seem to reach higher trophic levels as
735 no clear differences in meso-zooplankton abundances were observed between ambient and
736 warmed/acidified tanks at the end of the experiments. The duration of our experiments was too
737 short to carefully assess the proportion of newly formed organic matter consumed by meso-
738 zooplankton species and its effect on their biomass, yet group-specific variations were observed.

739 Finally, Gazeau et al. (2021) did not observe an additional impact of future environmental
740 conditions on the export of organic matter after dust addition.

5. Conclusion

These experiments conducted during the PEACETIME cruise represent the first attempt to investigate the impacts of atmospheric deposition on surface plankton communities both under present and future environmental conditions. Despite few experimental issues, the three experiments provided new insights on these potential impacts in the open Mediterranean Sea. Stark differences in the response to dust deposition were observed between the three investigated stations in the Tyrrhenian Sea, Ionian Sea and in the Algerian basin. Given that the initial conditions at the three stations were very similar in terms of nutrient and chlorophyll concentrations, these differences seem to be rather a consequence of the initial metabolic states of the community (autotrophy vs. heterotrophy). In all three cases, nutrient addition from dust deposition did not strongly modify but rather exacerbated this initial state. Relative changes in main parameters presented in this manuscript and processes presented in Gazeau et al. (2021) as a consequence of dust addition under present and future environmental conditions are shown in Fig. 10, and compared to the compilation of published data for the Mediterranean Sea from Guieu and Ridame (2020). At station TYR, under conditions of a clear dominance of heterotrophs on the use of resources and potentially a higher top-down control from grazers, dust addition drove the community into an even more heterotrophic state with no detectable effect on primary producers. At station ION, where the community was initially closer to metabolic balance, both heterotrophic and autotrophic compartments benefited from dust derived nutrients. At FAST, the station with the highest initial autotrophic production, addition of nutrients led to an increase in both compartments but heterotrophic prokaryotes became quickly P-limited and overall larger effects were observed for phytoplankton. Ocean acidification and warming did not have any detectable impact on the release of nutrients from atmospheric particles. Furthermore, these external drivers did not drastically modify the composition of the autotrophic assemblage

765 with all groups benefiting from warmer and acidified conditions. However, although for two out
766 of the three stations investigated, larger increases were observed for autotrophic as compared to
767 heterotrophic stocks under future environmental conditions, a stronger impact of warming and
768 acidification on mineralization processes (Gazeau et al., 2021) suggests that, in the future, the
769 plankton communities of Mediterranean surface waters will have a decreased capacity to
770 sequester atmospheric CO_2 following the deposition of atmospheric particles.

Data availability

All data and metadata will be made available at the French INSU/CNRS LEFE CYBER database (scientific coordinator: Hervé Claustre; data manager, webmaster: Catherine Schmechtig).

INSU/CNRS LEFE CYBER (2020)

Author contributions

FG and CG designed and supervised the study. FG, CG, CR and KD sampled seawater from the experimental tanks during the experiments. JMG and GDL participated in the technical preparation of the experimental system and all authors participated in sample analyses. FG, CR and CG wrote the paper with contributions from all authors.

Financial support

This study is a contribution to the PEACETIME project (http://peacetime-project.org), a joint initiative of the MERMEX and ChArMEx components supported by CNRS-INSU, IFREMER, CEA, and Météo-France as part of the programme MISTRALS coordinated by INSU. PEACETIME is a contribution to SOLAS and IMBER international programme. The project was endorsed as a process study by GEOTRACES. PEACETIME cruise (https://doi.org/10.17600/17000300). The project leading to this publication has also received funding from the European FEDER Fund under project 1166-39417.

Acknowledgments

The authors thank the captain and the crew of the RV Pourquoi Pas ? for their professionalism and their work at sea. We thank Julia Uitz, Céline Dimier and the SAPIGH HPLC analytical service at Institut de la Mer de Villefranche (IMEV) for sampling and analysis of phytoplankton pigments, John Dolan for microscopic countings as well as Lynne Macarez and the PIQv-

793 platform of EMBRC-France, a national Research Infrastructure supported by ANR, under the
794 reference ANR-10-INSB-02, for mesozooplankton analyses.

References

Aminot, A. and Kérouel, R.: Dosage automatique des nutriments dans les eaux marines : méthodes en flux continu, Editions Ifremer, méthodes d'analyse en milieu marin, 188 pp., 2007.

Behrenfeld, M. J., O'Malley, R. T., Siegel, D. A., McClain, C. R., Sarmiento, J. L., Feldman, G. C., Milligan, A. J., Falkowski, P. G., Letelier, R. M., and Boss, E. S.: Climate-driven trends in contemporary ocean productivity, Nature, 444, 752–755, 2006.

Bergametti, Gi., Dutot, A.-L., Buat-Ménard, P., Losno, R., and Remoudaki, E.: Seasonal variability of the elemental composition of atmospheric aerosol particles over the Northwestern Mediterranean, 41, 353–361, https://doi.org/10.3402/tellusb.v41i3.15092, 1989.

Bonnet, S. and Guieu, C.: Atmospheric forcing on the annual iron cycle in the western Mediterranean Sea: A 1-year survey, 111, https://doi.org/10.1029/2005JC003213, 2006.

Bonnet, S., Guieu, C., Chiaverini, J., Ras, J., and Stock, A.: Effect of atmospheric nutrients on the autotrophic communities in a low nutrient, low chlorophyll system, 50, 1810–1819, https://doi.org/10.4319/lo.2005.50.6.1810, 2005.

Børsheim, K. Y. and Bratbak, G.: Cell volume to cell carbon conversion factors for a bacterivorous Monas sp. enriched from seawater, 36, 171–175, 1987.

Bosc, E., Bricaud, A., and Antoine, D.: Seasonal and interannual variability in algal biomass and primary production in the Mediterranean Sea, as derived from 4 years of SeaWiFS observations, 18, https://doi.org/10.1029/2003GB002034, 2004.

Bressac, M. and Guieu, C.: Post-depositional processes: What really happens to new atmospheric iron in the ocean's surface?, 27, 859–870, https://doi.org/10.1002/gbc.20076, 2013.

Bressac, M., Guieu, C., Doxaran, D., Bourrin, F., Desboeufs, K., Leblond, N., and Ridame, C.: Quantification of the lithogenic carbon pump following a simulated dust-deposition event in large mesocosms, 11, 1007–1020, https://doi.org/10.5194/bg-11-1007-2014, 2014.

821 Bressac, M., Wagener, T., Leblond, N., Tovar-Sánchez, A., Ridame, C., Albani, S., Guasco, S.,
822 Dufour, A., Jacquet, S., Dulac, F., Desboeufs, K., and Guieu, C.: Subsurface iron
823 accumulation and rapid aluminium removal in the Mediterranean following African dust
824 deposition, Biogeosciences Discussions, 1–29, https://doi.org/10.5194/bg-2021-87, 2021.
825 Chen, B., Liu, H., Huang, B., and Wang, J.: Temperature effects on the growth rate of marine
826 picoplankton, 505, 37–47, https://doi.org/10.3354/meps10773, 2014.
827 Christaki, U., Courties, C., Massana, R., Catala, P., Lebaron, P., Gasol, J. M., and Zubkov, M.
828 V.: Optimized routine flow cytometric enumeration of heterotrophic flagellates using
829 SYBR Green I, 9, 329–339, https://doi.org/10.4319/lom.2011.9.329, 2011.
830 Daufresne, M., Lengfellner, K., and Sommer, U.: Global warming benefits the small in aquatic
831 ecosystems, PNAS, 106, 12788–12793, https://doi.org/10.1073/pnas.0902080106, 2009.
832 Desboeufs, K., Leblond, N., Wagener, T., Bon Nguyen, E., and Guieu, C.: Chemical fate and
833 settling of mineral dust in surface seawater after atmospheric deposition observed from
834 dust seeding experiments in large mesocosms, 11, 5581–5594, https://doi.org/10.5194/bg-
835 11-5581-2014, 2014.
836 Desboeufs, K., Bon Nguyen, E., Chevaillier, S., Triquet, S., and Dulac, F.: Fluxes and sources of
837 nutrient and trace metal atmospheric deposition in the Northwestern Mediterranean, 18,
838 14477–14492, https://doi.org/10.5194/acp-18-14477-2018, 2018.
839 Dickson, A. G., Sabine, C. L., and Christian, J. R.: Guide to best practices for ocean CO2
840 measurements, PICES, Sydney, 191 pp., 2007.
841 Dinasquet, J., Bigeard, E., Gazeau, F., Azam, F., Guieu, C., Marañón, E., Ridame, C., Van
842 Wambeke, F., Obernosterer, I., and Baudoux, A.-C.: Impact of dust addition on the
843 microbial food web under present and future conditions of pH and temperature,
844 Biogeosciences Discussions, 1–48, https://doi.org/10.5194/bg-2021-143, 2021.
845 Djaoudi, K., Van Wambeke, F., Coppola, L., D'Ortenzio, F., Helias-Nunige, S., Raimbault, P.,
846 Taillandier, V., Testor, P., Wagener, T., and Pulido-Villena, E.: Sensitive Determination of

847 the Dissolved Phosphate Pool for an Improved Resolution of Its Vertical Variability in the
848 Surface Layer: New Views in the P-Depleted Mediterranean Sea, Front. Mar. Sci., 5,
849 https://doi.org/10.3389/fmars.2018.00234, 2018.
850 D'Ortenzio, F., Iudicone, D., Montegut, C. de B., Testor, P., Antoine, D., Marullo, S., Santoleri,
851 R., and Madec, G.: Seasonal variability of the mixed layer depth in the Mediterranean Sea
852 as derived from in situ profiles, 32, https://doi.org/10.1029/2005GL022463, 2005.
853 Duce, R. A., Liss, P. S., Merrill, J. T., Atlas, E. L., Buat-Menard, P., Hicks, B. B., Miller, J. M.,
854 Prospero, J. M., Arimoto, R., Church, T. M., Ellis, W., Galloway, J. N., Hansen, L.,
855 Jickells, T. D., Knap, A. H., Reinhardt, K. H., Schneider, B., Soudine, A., Tokos, J. J.,
856 Tsunogai, S., Wollast, R., and Zhou, M.: The atmospheric input of trace species to the
857 world ocean, Global Biogeochemical Cycles, 5, 193–259,
858 https://doi.org/10.1029/91GB01778, 1991.
859 Dutkiewicz, S., Morris, J. J., Follows, M. J., Scott, J., Levitan, O., Dyhrman, S. T., and Berman-
860 Frank, I.: Impact of ocean acidification on the structure of future phytoplankton
861 communities, 5, 1002–1006, https://doi.org/10.1038/nclimate2722, 2015.
862 Emerson, S., Quay, P., Karl, D., Winn, C., Tupas, L., and Landry, M.: Experimental
863 determination of the organic carbon flux from open-ocean surface waters, 389, 951–954,
864 https://doi.org/10.1038/40111, 1997.
865 Falkovich, A. H., Ganor, E., Levin, Z., Formenti, P., and Rudich, Y.: Chemical and
866 mineralogical analysis of individual mineral dust particles, 106, 18029–18036,
867 https://doi.org/10.1029/2000JD900430, 2001.
868 Feliú, G., Pagano, M., Hidalgo, P., and Carlotti, F.: Structure and function of epipelagic
869 mesozooplankton and their response to dust deposition events during the spring
870 PEACETIME cruise in the Mediterranean Sea, 17, 5417–5441, https://doi.org/10.5194/bg-
871 17-5417-2020, 2020.

872 Gazeau, F., Van Wambeke, F., Marañón, E., Pérez-Lorenzo, M., Alliouane, S., Stolpe, C.,
873 Blasco, T., Leblond, N., Zäncker, B., Engel, A., Marie, B., Dinasquet, J., and Guieu, C.:
874 Impact of dust addition on the metabolism of Mediterranean plankton communities and
875 carbon export under present and future conditions of pH and temperature, Biogeosciences
876 Discussions, 1–74, https://doi.org/10.5194/bg-2021-20, 2021.
877 Gorsky, G., Ohman, M. D., Picheral, M., Gasparini, S., Stemmann, L., Romagnan, J.-B.,
878 Cawood, A., Pesant, S., García-Comas, C., and Prejger, F.: Digital zooplankton image
879 analysis using the ZooScan integrated system, J Plankton Res, 32, 285–303,
880 https://doi.org/10.1093/plankt/fbp124, 2010.
881 Guieu, C. and Ridame, C.: Impact of atmospheric deposition on marine chemistry and
882 biogeochemistry, in: Atmospheric Chemistry in the Mediterranean Region: Comprehensive
883 Diagnosis and Impacts, edited by: Dulac, F., Sauvage, S., and Hamonou, E., Springer,
884 Cham, Switzerland, 2020.
885 Guieu, C., Dulac, F., Desboeufs, K., Wagener, T., Pulido-Villena, E., Grisoni, J.-M., Louis, F.,
886 Ridame, C., Blain, S., Brunet, C., Bon Nguyen, E., Tran, S., Labiadh, M., and Dominici, J.-
887 M.: Large clean mesocosms and simulated dust deposition: a new methodology to
888 investigate responses of marine oligotrophic ecosystems to atmospheric inputs, 7, 2765–
889 2784, https://doi.org/10.5194/bg-7-2765-2010, 2010a.
890 Guieu, C., Loye-Pilot, M. D., Benyahya, L., and Dufour, A.: Spatial variability of atmospheric
891 fluxes of metals (Al, Fe, Cd, Zn and Pb) and phosphorus over the whole Mediterranean
892 from a one-year monitoring experiment: Biogeochemical implications, 120, 164–178,
893 https://doi.org/10.1016/j.marchem.2009.02.004, 2010b.
894 Guieu, C., Ridame, C., Pulido-Villena, E., Bressac, M., Desboeufs, K., and Dulac, F.: Impact of
895 dust deposition on carbon budget: a tentative assessment from a mesocosm approach, 11,
896 5621–5635, 2014a.

Guieu, C., Aumont, O., Paytan, A., Bopp, L., Law, C. S., Mahowald, N., Achterberg, E. P., Marañón, E., Salihoglu, B., Crise, A., Wagener, T., Herut, B., Desboeufs, K., Kanakidou, M., Olgun, N., Peters, F., Pulido-Villena, E., Tovar-Sanchez, A., and Völker, C.: The significance of the episodic nature of atmospheric deposition to Low Nutrient Low Chlorophyll regions, 28, 1179–1198, https://doi.org/10.1002/2014GB004852, 2014b.

Guieu, C., D'Ortenzio, F., Dulac, F., Taillandier, V., Doglioli, A., Petrenko, A., Barrillon, S., Mallet, M., Nabat, P., and Desboeufs, K.: Process studies at the air-sea interface after atmospheric deposition in the Mediterranean Sea: objectives and strategy of the PEACETIME oceanographic campaign (May–June 2017), 2020, 5563–5585, https://doi.org/10.5194/bg-17-5563-2020, 2020.

Herut, B., Zohary, T., Krom, M. D., Mantoura, R. F. C., Pitta, P., Psarra, S., Rassoulzadegan, F., Tanaka, T., and Frede Thingstad, T.: Response of East Mediterranean surface water to Saharan dust: On-board microcosm experiment and field observations, Deep Sea Research Part II: Topical Studies in Oceanography, 52, 3024–3040, https://doi.org/10.1016/j.dsr2.2005.09.003, 2005.

Holmes, R. M., Aminot, A., Kérouel, R., Hooker, B. A., and Peterson, B. J.: A simple and precise method for measuring ammonium in marine and freshwater ecosystems, Can. J. Fish. Aquat. Sci., 56, 1801–1808, https://doi.org/10.1139/f99-128, 1999.

IPCC: Climate Change, The Physical Science Basis, 2013.

IPCC: IPCC Special Report on the Ocean and Cryosphere in a Changing Climate, edited by: Pörtner, H. O., Roberts, D. C., Masson-Delmotte, V., Zhai, P., Tignor, M., Poloczanska, E., Mintenbeck, K., Alegría, A., Nicolai, M., Okem, A., Petzold, J., Rama, B., and Weyer, N. M., 2019.

Irwin, A. J. and Oliver, M. J.: Are ocean deserts getting larger?, 36, https://doi.org/10.1029/2009gl039883, 2009.

Jickells, T. D., An, Z. S., Andersen, K. K., Baker, A. R., Bergametti, G., Brooks, N., Cao, J. J., Boyd, P. W., Duce, R. A., Hunter, K. A., Kawahata, H., Kubilay, N., laRoche, J., Liss, P. S., Mahowald, N., Prospero, J. M., Ridgwell, A. J., Tegen, I., and Torres, R.: Global Iron Connections Between Desert Dust, Ocean Biogeochemistry, and Climate, 308, 67–71, https://doi.org/10.1126/science.1105959, 2005.

Kana, T. M. and Glibert, P. M.: Effect of irradiances up to 2000 μE m^{-2} s^{-1} on marine *Synechococcus* WH7803—I. Growth, pigmentation, and cell composition, Deep Sea Research Part A. Oceanographic Research Papers, 34, 479–495, https://doi.org/10.1016/0198-0149(87)90001-X, 1987.

Kapsenberg, L., Alliouane, S., Gazeau, F., Mousseau, L., and Gattuso, J.-P.: Coastal ocean acidification and increasing total alkalinity in the northwestern Mediterranean Sea, 13, 411–426, https://doi.org/10.5194/os-13-411-2017, 2017.

Kouvarakis, G., Mihalopoulos, N., Tselepides, A., and Stavrakakis, S.: On the importance of atmospheric inputs of inorganic nitrogen species on the productivity of the Eastern Mediterranean Sea, 15, 805–817, https://doi.org/10.1029/2001GB001399, 2001.

Lagaria, A., Mandalakis, M., Mara, P., Papageorgiou, N., Pitta, P., Tsiola, A., Kagiorgi, M., and Psarra, S.: Phytoplankton response to Saharan dust depositions in the Eastern Mediterranean Sea: A mesocosm study, Front. Mar. Sci., 3, https://doi.org/10.3389/fmars.2016.00287, 2017.

Law, C. S., Brévière, E., de Leeuw, G., Garçon, V., Guieu, C., Kieber, D. J., Kontradowitz, S., Paulmier, A., Quinn, P. K., Saltzman, E. S., Stefels, J., and von Glasow, R.: Evolving research directions in Surface Ocean - Lower Atmosphere (SOLAS) science, Environ. Chem., 10, 1, https://doi.org/10.1071/EN12159, 2013.

Lee, S. and Fuhrman, J. A.: Relationships between Biovolume and Biomass of Naturally Derived Marine Bacterioplankton, Appl Environ Microbiol, 53, 1298–1303, 1987.

947 Lekunberri, I., Lefort, T., Romero, E., Vázquez-Domínguez, E., Romera-Castillo, C., Marrasé,
948 C., Peters, F., Weinbauer, M., and Gasol, J. M.: Effects of a dust deposition event on
949 coastal marine microbial abundance and activity, bacterial community structure and
950 ecosystem function, J Plankton Res, 32, 381–396, https://doi.org/10.1093/plankt/fbp137,
951 2010.
952 Liu, X., Patsavas, M. C., and Byrne, R. H.: Purification and Characterization of meta-Cresol
953 Purple for Spectrophotometric Seawater pH Measurements, Environ. Sci. Technol., 45,
954 4862–4868, https://doi.org/10.1021/es200665d, 2011.
955 Longhurst, A., Sathyendranath, S., Platt, T., and Caverhill, C.: An estimate of global primary
956 production in the ocean from satellite radiometer data, 17, 1245–1271,
957 https://doi.org/10.1093/plankt/17.6.1245, 1995.
958 López-Urrutia, A. and Morán, X. A. G.: Resource limitation of bacterial production distorts the
959 temperature dependence of oceanic carbon cycling, Ecology, 88, 817–822,
960 https://doi.org/10.1890/06-1641, 2007.
961 Louis, J., Pedrotti, M. L., Gazeau, F., and Guieu, C.: Experimental evidence of formation of
962 transparent exopolymer particles (TEP) and POC export provoked by dust addition under
963 current and high pCO_2 conditions, PLOS ONE, 12, e0171980,
964 https://doi.org/10.1371/journal.pone.0171980, 2017a.
965 Louis, J., Guieu, C., and Gazeau, F.: Nutrient dynamics under different ocean acidification
966 scenarios in a low nutrient low chlorophyll system: The Northwestern Mediterranean Sea,
967 Estuarine, Coastal and Shelf Science, 186, 30–44,
968 https://doi.org/10.1016/j.ecss.2016.01.015, 2017b.
969 Louis, J., Gazeau, F., and Guieu, C.: Atmospheric nutrients in seawater under current and high
970 pCO_2 conditions after Saharan dust deposition: Results from three minicosm experiments,
971 Progress in Oceanography, 163, 40–49, https://doi.org/10.1016/j.pocean.2017.10.011,
972 2018.

973 Loÿe-Pilot, M. D. and Martin, J. M.: Saharan Dust Input to the Western Mediterranean: An
974 Eleven Years Record in Corsica, in: The Impact of Desert Dust Across the Mediterranean,
975 edited by: Guerzoni, S. and Chester, R., Springer Netherlands, Dordrecht, 191–199,
976 https://doi.org/10.1007/978-94-017-3354-0_18, 1996.
977 Manca, B., Burca, M., Giorgetti, A., Coatanoan, C., Garcia, M.-J., and Iona, A.: Physical and
978 biochemical averaged vertical profiles in the Mediterranean regions: an important tool to
979 trace the climatology of water masses and to validate incoming data from operational
980 oceanography, Journal of Marine Systems, 48, 83–116,
981 https://doi.org/10.1016/j.jmarsys.2003.11.025, 2004.
982 Marañón, E., Fernández, A., Mouriño-Carballido, B., MartÍnez-GarcÍa, S., Teira, E., Cermeño,
983 P., Chouciño, P., Huete-Ortega, M., Fernández, E., Calvo-DÍaz, A., Morán, X. A. G.,
984 Bode, A., Moreno-Ostos, E., Varela, M. M., Patey, M. D., and Achterberg, E. P.: Degree of
985 oligotrophy controls the response of microbial plankton to Saharan dust, 55, 2339–2352,
986 https://doi.org/10.4319/lo.2010.55.6.2339, 2010.
987 Marañón, E., Lorenzo, M. P., Cermeño, P., and Mouriño-Carballido, B.: Nutrient limitation
988 suppresses the temperature dependence of phytoplankton metabolic rates, 12, 1836–1845,
989 https://doi.org/10.1038/s41396-018-0105-1, 2018.
990 Marie, D., Simon, N., Guillou, L., Partensky, F., and Vaulot, D.: Flow cytometry analysis of
991 marine picoplankton, in: living color: protocols in flow cytometry and cell sorting, edited
992 by: Diamond, R. A. and DeMaggio, S., Springer, Berlin, 421–454, 2010.
993 Markaki, Z., Oikonomou, K., Kocak, M., Kouvarakis, G., Chaniotaki, A., Kubilay, N., and
994 Mihalopoulos, N.: Atmospheric deposition of inorganic phosphorus in the Levantine Basin,
995 eastern Mediterranean: Spatial and temporal variability and its role in seawater
996 productivity, 48, 1557–1568, https://doi.org/10.4319/lo.2003.48.4.1557, 2003.

997 Maugendre, L., Gattuso, J.-P., Louis, J., de Kluijver, A., Marro, S., Soetaert, K., and Gazeau, F.:
998 Effect of ocean warming and acidification on a plankton community in the NW
999 Mediterranean Sea, 72, 1744–1755, https://doi.org/10.1093/icesjms/fsu161, 2015.
1000 Maugendre, L., Guieu, C., Gattuso, J.-P., and Gazeau, F.: Ocean acidification in the
1001 Mediterranean Sea: Pelagic mesocosm experiments. A synthesis, Estuarine, Coastal and
1002 Shelf Science, 186, 1–10, https://doi.org/10.1016/j.ecss.2017.01.006, 2017.
1003 Mayot, N., D'Ortenzio, F., Ribera d'Alcalà, M., Lavigne, H., and Claustre, H.: Interannual
1004 variability of the Mediterranean trophic regimes from ocean color satellites, 13, 1901–
1005 1917, https://doi.org/10.5194/bg-13-1901-2016, 2016.
1006 Mélançon, J., Levasseur, M., Lizotte, M., Scarratt, M., Tremblay, J.-É., Tortell, P., Yang, G.-P.,
1007 Shi, G.-Y., Gao, H., Semeniuk, D., Robert, M., Arychuk, M., Johnson, K., Sutherland, N.,
1008 Davelaar, M., Nemcek, N., Peña, A., and Richardson, W.: Impact of ocean acidification on
1009 phytoplankton assemblage, growth, and DMS production following Fe-dust additions in
1010 the NE Pacific high-nutrient, low-chlorophyll waters, 13, 1677–1692,
1011 https://doi.org/10.5194/bg-13-1677-2016, 2016.
1012 Moore, C. M., Mills, M. M., Arrigo, K. R., Berman-Frank, I., Bopp, L., Boyd, P. W., Galbraith,
1013 E. D., Geider, R. J., Guieu, C., Jaccard, S. L., Jickells, T. D., La Roche, J., Lenton, T. M.,
1014 Mahowald, N. M., Marañón, E., Marinov, I., Moore, J. K., Nakatsuka, T., Oschlies, A.,
1015 Saito, M. A., Thingstad, T. F., Tsuda, A., and Ulloa, O.: Processes and patterns of oceanic
1016 nutrient limitation, 6, 701–710, https://doi.org/10.1038/ngeo1765, 2013.
1017 Morán, X. A. G., López-Urrutia, Á., Calvo-Díaz, A., and Li, W. K. W.: Increasing importance of
1018 small phytoplankton in a warmer ocean, 16, 1137–1144, https://doi.org/10.1111/j.1365-
1019 2486.2009.01960.x, 2010.
1020 Neale, P. J., Sobrino, C., Segovia, M., Mercado, J. M., Leon, P., Cortés, M. D., Tuite, P., Picazo,
1021 A., Salles, S., Cabrerizo, M. J., Prasil, O., Montecino, V., Reul, A., and Fuentes-Lema, A.:

Effect of CO2, nutrients and light on coastal plankton. I. Abiotic conditions and biological responses, 22, 25–41, https://doi.org/10.3354/ab00587, 2014.

Obernosterer, I., Kawasaki, N., and Benner, R.: P-limitation of respiration in the Sargasso Sea and uncoupling of bacteria from P-regeneration in size-fractionation experiments, 32, 229–237, https://doi.org/10.3354/ame032229, 2003.

Orr, J. C., Epitalon, J.-M., Dickson, A. G., and Gattuso, J.-P.: Routine uncertainty propagation for the marine carbon dioxide system, 207, 84–107, https://doi.org/10.1016/j.marchem.2018.10.006, 2018.

Paytan, A., Mackey, K. R. M., Chen, Y., Lima, I. D., Doney, S. C., Mahowald, N., Labiosa, R., and Post, A. F.: Toxicity of atmospheric aerosols on marine phytoplankton, 106, 4601–4605, https://doi.org/10.1073/pnas.0811486106, 2009.

Pitta, P., Kanakidou, M., Mihalopoulos, N., Christodoulaki, S., Dimitriou, P. D., Frangoulis, C., Giannakourou, A., Kagiorgi, M., Lagaria, A., Nikolaou, P., Papageorgiou, N., Psarra, S., Santi, I., Tsapakis, M., Tsiola, A., Violaki, K., and Petihakis, G.: Saharan Dust Deposition Effects on the Microbial Food Web in the Eastern Mediterranean: A Study Based on a Mesocosm Experiment, Front. Mar. Sci., 4, https://doi.org/10.3389/fmars.2017.00117, 2017.

Polovina, J. J., Howell, E. A., and Abecassis, M.: Ocean’s least productive waters are expanding, 35, https://doi.org/10.1029/2007gl031745, 2008.

Powley, H. R., Krom, M. D., and Cappellen, P. V.: Understanding the unique biogeochemistry of the Mediterranean Sea: Insights from a coupled phosphorus and nitrogen model, 31, 1010–1031, https://doi.org/10.1002/2017GB005648, 2017.

Pulido-Villena, E., Wagener, T., and Guieu, C.: Bacterial response to dust pulses in the western Mediterranean: Implications for carbon cycling in the oligotrophic ocean, 22, https://doi.org/10.1029/2007gb003091, 2008.

1047 Pulido-Villena, E., Rerolle, V., and Guieu, C.: Transient fertilizing effect of dust in P-deficient
1048 LNLC surface ocean, 37, https://doi.org/10.1029/2009gl041415, 2010.
1049 Pulido-Villena, E., Baudoux, A.-C., Obernosterer, I., Landa, M., Caparros, J., Catala, P.,
1050 Georges, C., Harmand, J., and Guieu, C.: Microbial food web dynamics in response to a
1051 Saharan dust event: results from a mesocosm study in the oligotrophic Mediterranean Sea,
1052 11, 5607–5619, 2014.
1053 Putaud, J.-P., Dingenen, R. V., Dell'Acqua, A., Raes, F., Matta, E., Decesari, S., Facchini, M. C.,
1054 and Fuzzi, S.: Size-segregated aerosol mass closure and chemical composition in Monte
1055 Cimone (I) during MINATROC, 4, 889–902, https://doi.org/10.5194/acp-4-889-2004,
1056 2004.
1057 Ras, J., Claustre, H., and Uitz, J.: Spatial variability of phytoplankton pigment distributions in
1058 the Subtropical South Pacific Ocean: comparison between in situ and predicted data, 5,
1059 353–369, https://doi.org/10.5194/bg-5-353-2008, 2008.
1060 Regaudie-de-Gioux, A., Vaquer-Sunyer, R., and Duarte, C. M.: Patterns in planktonic
1061 metabolism in the Mediterranean Sea, 6, 3081–3089, https://doi.org/10.5194/bg-6-3081-
1062 2009, 2009.
1063 Richon, C., Dutay, J.-C., Dulac, F., Wang, R., Balkanski, Y., Nabat, P., Aumont, O., Desboeufs,
1064 K., Laurent, B., Guieu, C., Raimbault, P., and Beuvier, J.: Modeling the impacts of
1065 atmospheric deposition of nitrogen and desert dust-derived phosphorus on nutrients and
1066 biological budgets of the Mediterranean Sea, Progress in Oceanography, 163, 21–39,
1067 https://doi.org/10.1016/j.pocean.2017.04.009, 2018.
1068 Ridame, C. and Guieu, C.: Saharan input of phosphate to the oligotrophic water of the open
1069 western Mediterranean Sea, 47, 856–869, 2002.
1070 Ridame, C., Guieu, C., and L'Helguen, S.: Strong stimulation of N 2 fixation in oligotrophic
1071 Mediterranean Sea: results from dust addition in large in situ mesocosms, 10, 7333–7346,
1072 2013.

Ridame, C., Dekaezemacker, J., Guieu, C., Bonnet, S., L'Helguen, S., and Malien, F.: Contrasted Saharan dust events in LNLC environments: impact on nutrient dynamics and primary production, 11, 4783–4800, 2014.

Romero, E., Peters, F., Marrasé, C., Guadayol, Ò., Gasol, J. M., and Weinbauer, M. G.: Coastal Mediterranean plankton stimulation dynamics through a dust storm event: An experimental simulation, Estuarine, Coastal and Shelf Science, 93, 27–39, https://doi.org/10.1016/j.ecss.2011.03.019, 2011.

Roy-Barman, M., Foliot, L., Douville, E., Leblond, N., Gazeau, F., Bressac, M., Wagener, T., Ridame, C., Desboeufs, K., and Guieu, C.: Contrasted release of insoluble elements (Fe, Al, rare earth elements, Th, Pa) after dust deposition in seawater: a tank experiment approach, Biogeosciences, 18, 2663–2678, https://doi.org/10.5194/bg-18-2663-2021, 2021.

Sala, M. M., Aparicio, F. L., Balagué, V., Boras, J. A., Borrull, E., Cardelús, C., Cros, L., Gomes, A., López-Sanz, A., Malits, A., Martínez, R. A., Mestre, M., Movilla, J., Sarmento, H., Vázquez-Domínguez, E., Vaqué, D., Pinhassi, J., Calbet, A., Calvo, E., Gasol, J. M., Pelejero, C., and Marrasé, C.: Contrasting effects of ocean acidification on the microbial food web under different trophic conditions, 73, 670–679, https://doi.org/10.1093/icesjms/fsv130, 2016.

Sherr, E. B. and Sherr, B. F.: Bacterivory and herbivory: Key roles of phagotrophic protists in pelagic food webs, Microb Ecol, 28, 223–235, https://doi.org/10.1007/BF00166812, 1994.

Siokou-Frangou, I., Christaki, U., Mazzocchi, M. G., Montresor, M., Ribera d'Alcalá, M., Vaqué, D., and Zingone, A.: Plankton in the open Mediterranean Sea: a review, 7, 1543–1586, https://doi.org/10.5194/bg-7-1543-2010, 2010.

Tanaka, T., Thingstad, T. F., Christaki, U., Colombet, J., Cornet-Barthaux, V., Courties, C., Grattepanche, J.-D., Lagaria, A., Nedoma, J., Oriol, L., Psarra, S., Pujo-Pay, M., and Wambeke, F. V.: Lack of P-limitation of phytoplankton and heterotrophic prokaryotes in

surface waters of three anticyclonic eddies in the stratified Mediterranean Sea, 8, 525–538, https://doi.org/10.5194/bg-8-525-2011, 2011.

Ternon, E., Guieu, C., Loÿe-Pilot, M.-D., Leblond, N., Bosc, E., Gasser, B., Miquel, J.-C., and Martín, J.: The impact of Saharan dust on the particulate export in the water column of the North Western Mediterranean Sea, 7, 809–826, https://doi.org/10.5194/bg-7-809-2010, 2010.

The Mermex group: Marine ecosystems' responses to climatic and anthropogenic forcings in the Mediterranean, 91, 97–166, https://doi.org/10.1016/j.pocean.2011.02.003, 2011.

Theodosi, C., Markaki, Z., Tselepides, A., and Mihalopoulos, N.: The significance of atmospheric inputs of soluble and particulate major and trace metals to the eastern Mediterranean seawater, Marine Chemistry, 120, 154–163, https://doi.org/10.1016/j.marchem.2010.02.003, 2010.

Van Wambeke, F., Goutx, M., Striby, L., Sempéré, R., and Vidussi, F.: Bacterial dynamics during the transition from spring bloom to oligotrophy in the northwestern Mediterranean Sea: relationships with particulate detritus and dissolved organic matter, 212, 89–105, 2001.

Van Wambeke, F., Taillandier, V., Deboeufs, K., Pulido-Villena, E., Dinasquet, J., Engel, A., Marañón, E., Ridame, C., and Guieu, C.: Influence of atmospheric deposition on biogeochemical cycles in an oligotrophic ocean system, 1–51, https://doi.org/10.5194/bg-2020-411, 2020a.

Van Wambeke, F., Pulido, E., Dinasquet, J., Djaoudi, K., Engel, A., Garel, M., Guasco, S., Nunige, S., Taillandier, V., Zäncker, B., and Tamburini, C.: Spatial patterns of biphasic ectoenzymatic kinetics related to biogeochemical properties in the Mediterranean Sea, 1–38, https://doi.org/10.5194/bg-2020-253, 2020b.

Verity, P. G., Robertson, C. Y., Tronzo, C. R., Andrews, M. G., Nelson, J. R., and Sieracki, M. E.: Relationships between cell volume and the carbon and nitrogen content of marine

photosynthetic nanoplankton, 37, 1434–1446, https://doi.org/10.4319/lo.1992.37.7.1434, 1992.

Vidussi, F., Claustre, H., Manca, B. B., Luchetta, A., and Marty, J.-C.: Phytoplankton pigment distribution in relation to upper thermocline circulation in the eastern Mediterranean Sea during winter, 106, 19939–19956, https://doi.org/10.1029/1999JC000308, 2001.

Table 1. List of parameters and processes investigated during the three experiments at stations TYR, ION and FAST. Corresponding manuscripts are indicated. pH_T: pH on the total scale, A_T: total alkalinity, ^{13}C-C_T: ^{13}C signature of dissolved inorganic carbon, NO_x: nitrate + nitrite, DIP: dissolved inorganic phosphorus, $Si(OH)_4$: silicate, DFe: dissolved iron, DAl: dissolved aluminium, Th-REE-Pa: Thorium (^{230}Th and ^{232}Th), Rare Earth elements and Protactinium (^{231}Pa), POC: particulate organic carbon, DOC: dissolved organic carbon, ^{13}C-DOC: ^{13}C signature of dissolved organic carbon, TEP: transparent exopolymer particles, NCP/CR: net community production and community respiration (oxygen based), ^{14}C-PP: primary production based on ^{14}C incorporation.

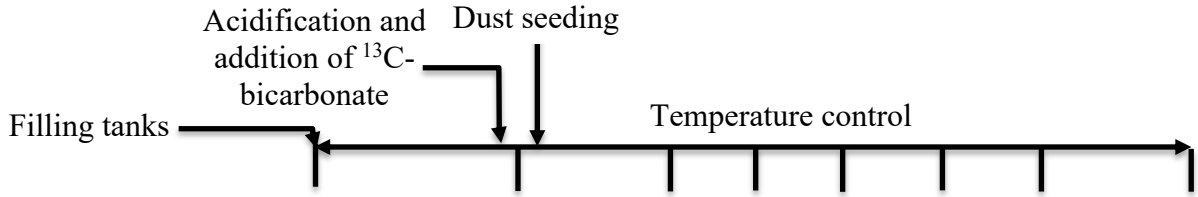

Sampling time	t-12h	t0	t1h	t6h	t12h	t24h	t48h	t72h / t96h	Related manuscript
	Hours post dust seeding								
Temperature	Continuous								This manuscript
Irradiance	Continuous								This manuscript

Carbonate chemistry

pH_T		This manuscript
A_T		This manuscript
$\delta^{13}C$-C_T		Gazeau et al. (2021)

Macro-nutrients

NO_x		This manuscript
DIP		This manuscript
$Si(OH)_4$		This manuscript

Micro-nutrients

DFe		Roy-Barman et al. (2021)
DAl		Roy-Barman et al. (2021)
Th-REE-Pa		Roy-Barman et al. (2021)

Biological stocks

Pigments		This manuscript
Flow cytometry		This manuscript

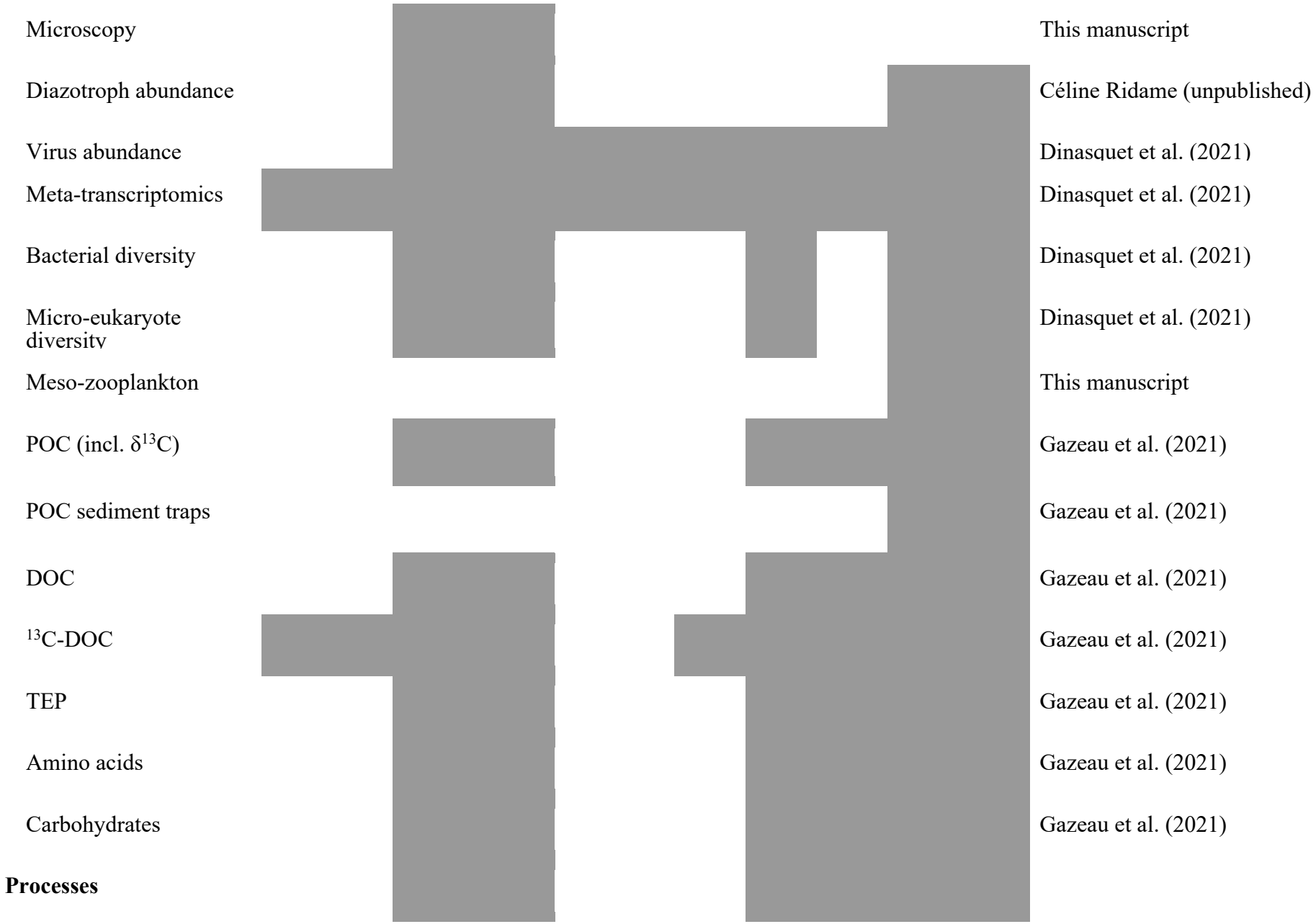
Microscopy
This manuscript
Diazotroph abundance
Céline Ridame (unpublished)
Virus abundance
Dinasquet et al. (2021)
Meta-transcriptomics
Dinasquet et al. (2021)
Bacterial diversity
Dinasquet et al. (2021)
Micro-eukaryote diversity
Dinasquet et al. (2021)
Meso-zooplankton
This manuscript
POC (incl. δ13C)
Gazeau et al. (2021)
POC sediment traps
Gazeau et al. (2021)
DOC
Gazeau et al. (2021)
13C-DOC
Gazeau et al. (2021)
TEP
Gazeau et al. (2021)
Amino acids
Gazeau et al. (2021)
Carbohydrates
Gazeau et al. (2021)
Processes

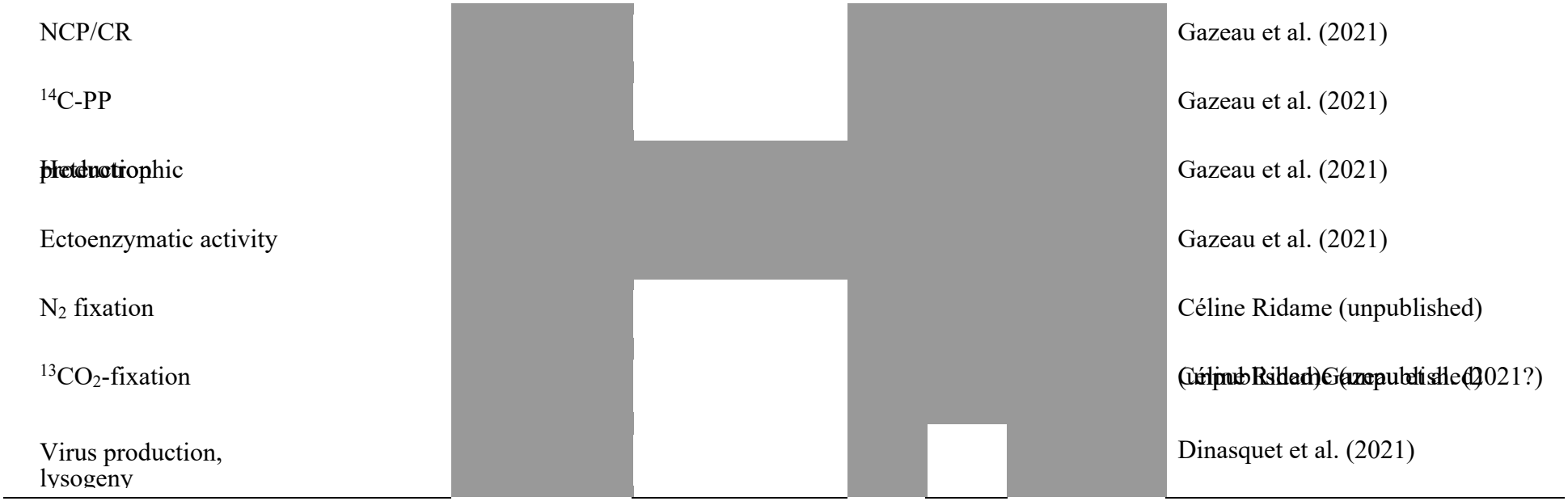
NCP/CR
Gazeau et al. (2021)
^{14}C-PP
Gazeau et al. (2021)
Heterotrophic production
Gazeau et al. (2021)
Ectoenzymatic activity
Gazeau et al. (2021)
N_2 fixation
Céline Ridame (unpublished)
$^{13}CO_2$-fixation
Céline Ridame (unpublished)
Virus production, lysogeny
Dinasquet et al. (2021)

1142

Table 2. Initial conditions (sampling time t-12h) at stations TYR, ION and FAST measured while filling the tanks. pH_T: pH on the total scale, NO_x: nitrate + nitrite, NH_4: ammonium, DIP: dissolved inorganic phosphorus, $Si(OH)_4$: silicate, TChl*a*: total chlorophyll *a*, HNF: heterotrophic nanoflagellates. The three most important pigments in terms of concentration are also presented (19'-hexanoyloxyfucoxanthin, Zeaxanthin and Divinyl Chlorophyll *a*). Biomasses of the different groups analyzed through flow cytometry were estimated based on conversion equations and/or factors found in the literature (see section 2.3). Autotrophic and heterotrophic biomass based on flow cytometry (fraction < 20 µm). Values below detection limits are indicated as < dl.

	Sampling station	TYR	ION	FAST
	Coordinates (decimal)	39.34 N, 12.60 E	35.49 N, 19.78 E	37.95 N, 2.90 N
	Bottom depth (m)	3395	3054	2775
	Day and time of sampling (local time)	17/05/2017 17:00	25/05/2017 17:00	02/06/2017 21:00
	Temperature (°C)	20.6	21.2	21.5
	Salinity	37.96	39.02	37.07
Carbonate chemistry	pH_T	8.04	8.07	8.03
	Total alkalinity (µmol kg^{-1})	2529	2627	2443
Nutrients	NO_x (nmol L^{-1})	14.0	18.0	59.0

	NH_4^+ (µmol L^{-1})	0.045	0.022	< dl
	DIP (nmol L^{-1})	17.1	6.5	12.9
	$Si(OH)_4$ (µmol L^{-1})	1.0	0.96	0.64
	NO_x/DIP (molar ratio)	0.8	2.5	4.6
Pigments	TChl*a* (µg L^{-1})	0.063	0.066	0.072
	19'-hexanoyloxyfucoxanthin (µg L^{-1})	0.017	0.021	0.016
	Zeaxanthin (µg L^{-1})	0.009	0.006	0.036
	Divinyl Chlorophyll *a* (µg L^{-1})	~ 0	0	0.014
Flow cytometry	Autotrophic pico-eukaryotes (cell mL^{-1}; biomass in µg C L^{-1})	347.8; 0.5	239.9; 0.4	701.0; 1.0
	Autotrophic nano-eukaryotes (cell mL^{-1}; biomass in µg C L^{-1})	150.5; 3.9	188.8; 4.8	196.6; 5.0
	Synechococcus (cell mL^{-1}; biomass in µg C L^{-1})	4972; 1.2	3037; 0.8	6406; 1.6
	Autotrophic biomass (µg C L^{-1})	5.6	6.0	7.7
	Heterotrophic prokaryotes abundance (x 10^5 cell mL^{-1})	4.79	2.14	6.15
	HNF (abundance in cell mL^{-1})	110.1	53.6	126.2
	Heterotrophic biomass (µg C L^{-1})	9.9	4.5	12.7
Microscopy	Pennate diatoms (abundance in cell L^{-1})	140	520	880
	Centric diatoms (abundance in cell L^{-1})	200	380	580
	Dinoflagellates (abundance in cell L^{-1})	2770	3000	3410
	Autotrophic flagellates (abundance in cell L^{-1})	0	60	650

Ciliates (abundance in cell L^{-1})	270	380	770

1152

Table 3. Maximum input of nitrate + nitrite (NO_x) and dissolved inorganic phosphorus (DIP) released from Saharan dust in tanks D and G as observed from the discrete samples taken during the first 6 h after seeding. The estimated maximal percentage of dissolution is also presented (see section 2.3.1 for details on the calculations).

	NO_x				DIP			
	D1	D2	G1	G2	D1	D2	G1	G2
Maximum input			$\mu mol\ L^{-1}$				$nmol\ L^{-1}$	
TYR	11.0	11.1	11.1	11.0	24.6	20.4	24.6	23.9
ION	11.2	11.6	11.2	11.3	23.3	22.0	19.6	22.9
FAST	11.3	11.1	11.1	11.2	30.8	31.3	36.9	29.8
Maximum dissolution (%)								
TYR	95	96	95	94	12	10	12	11
ION	96	99	96	97	11	10	9	11
FAST	97	97	95	97	15	15	17	14

Table 4. Removal rate of nitrate + nitrite (NO_x) and dissolved inorganic phosphorus (DIP) in tanks D and G during the three experiments (TYR, ION and FAST). For NO_x, rates were estimated based on linear regressions between maximum concentrations (i.e. after dust enrichment, at t1h or t6h) and final concentrations (t72 h for TYR and ION and t96h for FAST). For DIP, rates were estimated based on linear regressions between maximum concentrations (i.e. after dust enrichment at t1h or t6h) and concentrations after stabilization was observed. This sampling time is shown in parentheses. All rates are expressed in nmol L^{-1} h^{-1}.

	NO_x			DIP		
	TYR	ION	FAST	TYR	ION	FAST
D1	-6.5	-8.6	-14.3	-0.4 (t72h)	-0.5 (t48h)	-0.2 (t96h)
D2	-1.0	-8.6	-13.5	-0.3 (t72h)	-0.8 (t24h)	-0.2 (t96h)
G1	-6.7	-13.1	-21.6	-1.3 (t24h)	-0.8 (t24h)	-1.5 (t24h)
G2	-0.8	-1.6	-25.2	-1.3 (t24h)	-1.6 (t24h)	-1.1 (t24h)

Table 5. Percent (%) maximum relative changes in tanks D and G as compared to controls (average between C1 and C2), for the experiments TYR, ION and FAST. The sampling time at which these maximum relative changes were observed is shown in brackets. Tchl*a* refers to the concentration of total chlorophyll *a* and B_{micro} to the biomass proxy of micro-phytoplankton (sum of Fucoxanthin and Peridinin, see Material and Methods) based on high performance liquid chromatography (HPLC). HP and HNF refer to heterotrophic prokaryote and heterotrophic nanoflagellate abundances, respectively, measured by flow cytometry.

Experiment	Tank	HPLC		Flow cytometry				
		TChl*a*	B_{micro}	Autotrophic Pico-eukaryotes	Autotrophic Nano-eukaryotes	*Synechococcus*	HP	HNF
TYR	D1	-35 (t24h)	-33 (t12h)	-75 (t72h)	-80 (t1h)	-71 (t48h)	68 (t72h)	352 (t72h)
TYR	D2	-38 (t12h)	-39 (t24h)	-75 (t72h)	-80 (t1h)	-72 (t48h)	53 (t72h)	100 (t72h)
TYR	G1	60 (t72h)	52 (t72h)	-75 (t1h)	89 (t72h)	76 (t72h)	67 (t72h)	1095 (t72h)
TYR	G2	359 (t72h)	392 (t72h)	323 (t72h)	119 (t72h)	700 (t72h)	68 (t48h)	298 (t72h)
ION	D1	183 (t72h)	157 (t72h)	126 (t72h)	89 (t72h)	317 (t72h)	128 (t72h)	44 (t72h)

ION	D2	109 (t72h)	156 (t72h)	117 (t72h)	-59 (t1h)	390 (t72h)	133 (t72h)	27 (t72h)
ION	G1	399 (t72h)	454 (t72h)	458 (t72h)	256 (t72h)	805 (t72h)	176 (t72h)	175 (t72h)
ION	G2	426 (t72h)	612 (t72h)	510 (t72h)	292 (t72h)	1425 (t72h)	161 (t72h)	129 (t72h)
FAST	D1	318 (t96h)	356 (t96h)	113 (t96h)	208 (t72h)	348 (t96h)	27 (t96h)	-38 (t96h)
FAST	D2	237 (t96h)	322 (t96h)	91 (t96h)	219 (t72h)	197 (t96h)	40 (t48h)	-49 (t96h)
FAST	G1	399 (t96h)	415 (t96h)	198 (t72h)	274 (t72h)	357 (t48h)	61 (t48h)	243 (t24h)
FAST	G2	395 (t96h)	421 (t96h)	129 (t72h)	202 (t96h)	344 (t48h)	67 (t48h)	74 (t24h)

Figure captions

Fig. 1. Location of the sampling stations in the Mediterranean Sea onboard the R/V "Pourquoi Pas ?" during the PEACETIME cruise. Background shows satellite-derived surface chlorophyll *a* concentration averaged over the entire duration of the cruise (Courtesy of Louise Rousselet).

Fig. 2. Diagram of an experimental tank (climate reactor).

Fig. 3. Proportion of the different pigments, as measured by high performance liquid chromatography (HPLC) in pumped surface seawater for the three experiments (t-12h).

Fig. 4. Continuous measurements of temperature and irradiance level (PAR) in the six tanks during the experiments at TYR, ION and FAST. The dashed vertical line indicates the time of dust seeding (after t0).

Fig. 5. pH on the total scale (pH_T) and total alkalinity (A_T) measured in the six tanks during the experiments at TYR, ION and FAST. The dashed vertical line indicates the time of dust seeding (after t0). Error bars correspond to the standard deviation based on analytical triplicates.

Fig. 6. Nutrients (nitrate + nitrite): NO_x, dissolved inorganic phosphorus: DIP, silicate: $Si(OH)_4$ and the molar ratio between NO_x and DIP, measured in each tank during the experiments at TYR, ION and FAST. The dashed vertical line indicates the time of seeding (after t0).

Fig. 7. Total chlorophyll *a* and major pigments, from high performance liquid chromatography (HPLC) measurements, in each tank during the experiments at TYR, ION and FAST. The dashed vertical line indicates the time of seeding (after t0).

Fig. 8. Abundance of autotrophic pico-eukaryotes, autotrophic nano-eukaryotes, *Synechococcus,* heterotrophic prokaryotes (HP), and heterotrophic nano-flagellates (HNF), measured by flow cytometry, in each tank during the experiments at TYR, ION and FAST. The evolution of

autotrophic biomass (see Material and Methods for details on the calculation) is also shown. The dashed vertical line indicates the time of seeding (after t0).

Fig. 9. Abundances of meso-zooplankton species as measured in each tank at the end of the experiments at TYR, ION and FAST.

Fig. 10. Maximum relative change (%) of main biological stocks (TCHl*a*: total chlorophyll *a*, HP: heterotrophic prokaryotes) and processes (BP: bacterial production; PP: ^{14}C-based primary production; see Gazeau et al., 2021; BR: bacterial respiration (no data from this study); and N_2 fixation, Céline Ridame, unpublished results) obtained during the present study at the three stations (TYR, ION and FAST) under ambient conditions of pH and temperature (open red squares) and future conditions (full green squares). Vertical extension of each squares are delimited by the range of responses observed among the duplicates for each treatment. The dotted green squares for station TYR highlight the large variability observed between duplicates for some parameters and processes that prevented drawing solid conclusions. Box-plots (Med) represent the distribution of responses observed from studies conducted in the Mediterranean Sea, as compiled by Guieu and Ridame (2020).

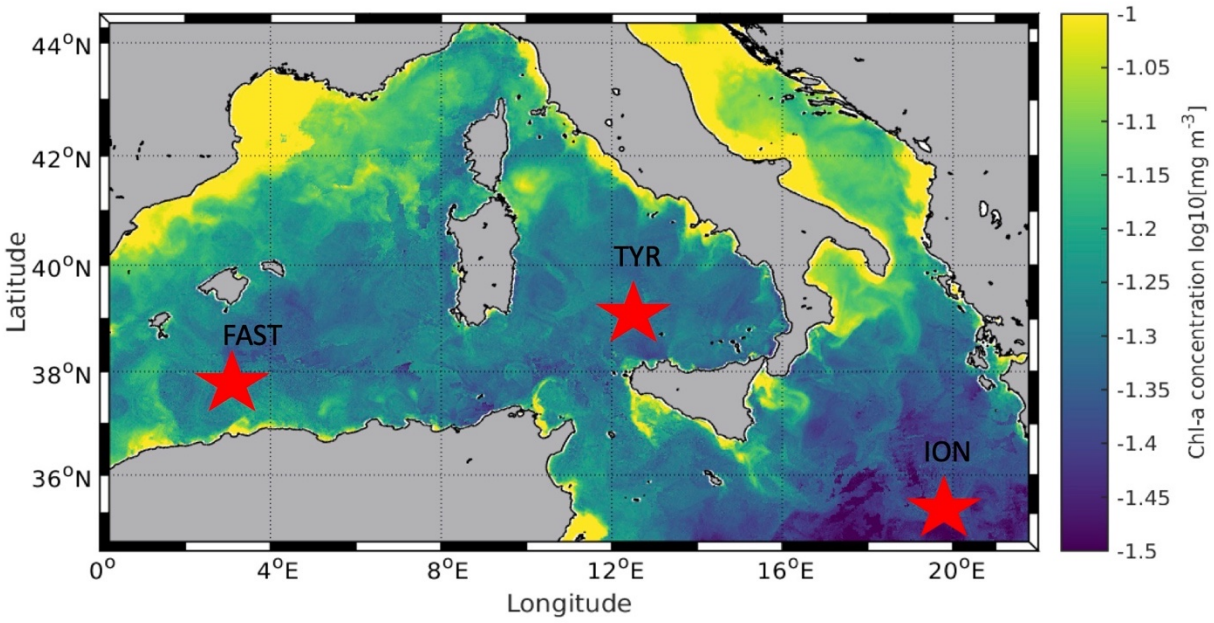
44°N
42°N
40°N
38°N
36°N
Latitude
0°
4°E
8°E
12°E
16°E
20°E
Longitude
FAST
TYR
ION
-1
-1.05
-1.1
-1.15
-1.2
-1.25
-1.3
-1.35
-1.4
-1.45
-1.5
Chl-a concentration log10[mg m-3]

Fig. 1.

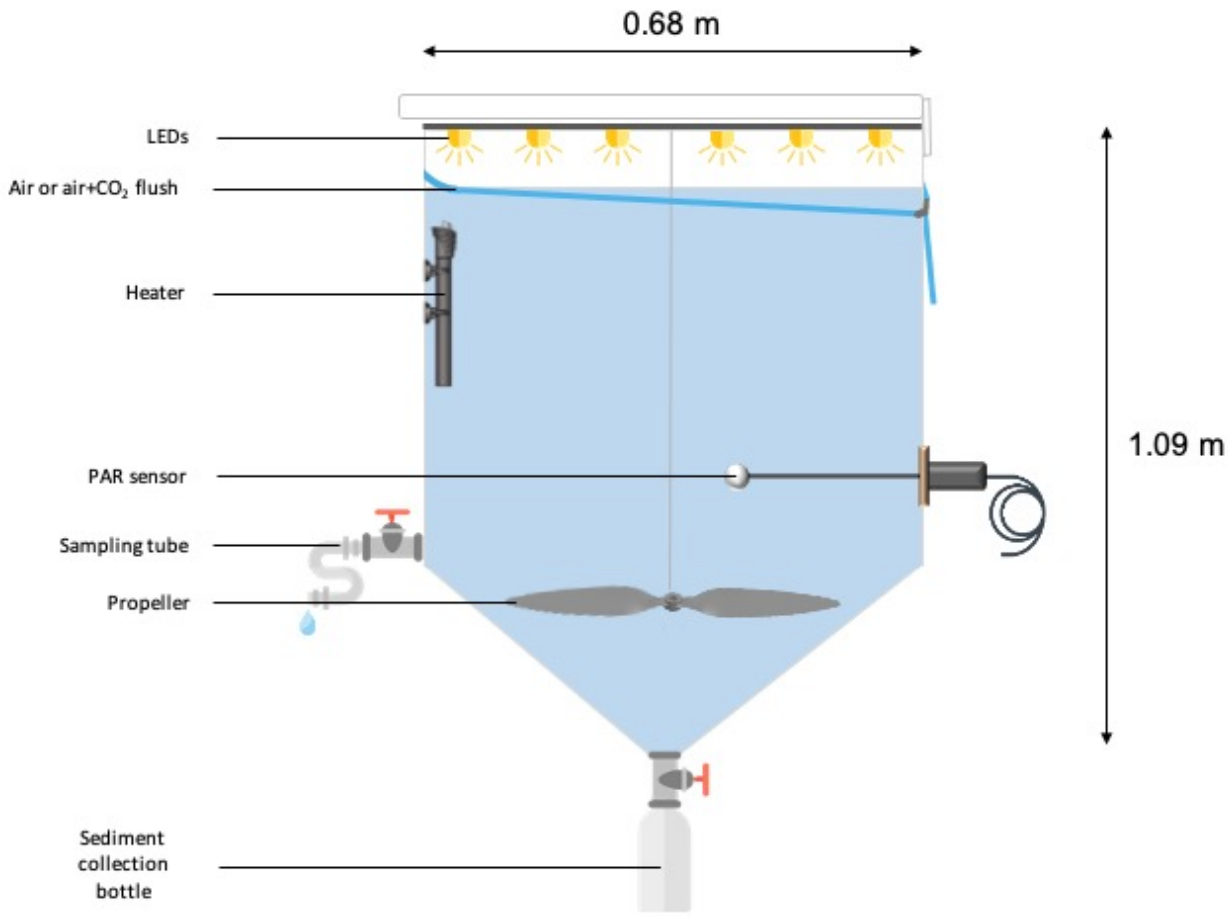
0.68 m
LEDs
Air or air+CO_2 flush
Heater
PAR sensor
Sampling tube
Propeller
Sediment collection bottle
1.09 m

Fig. 2.

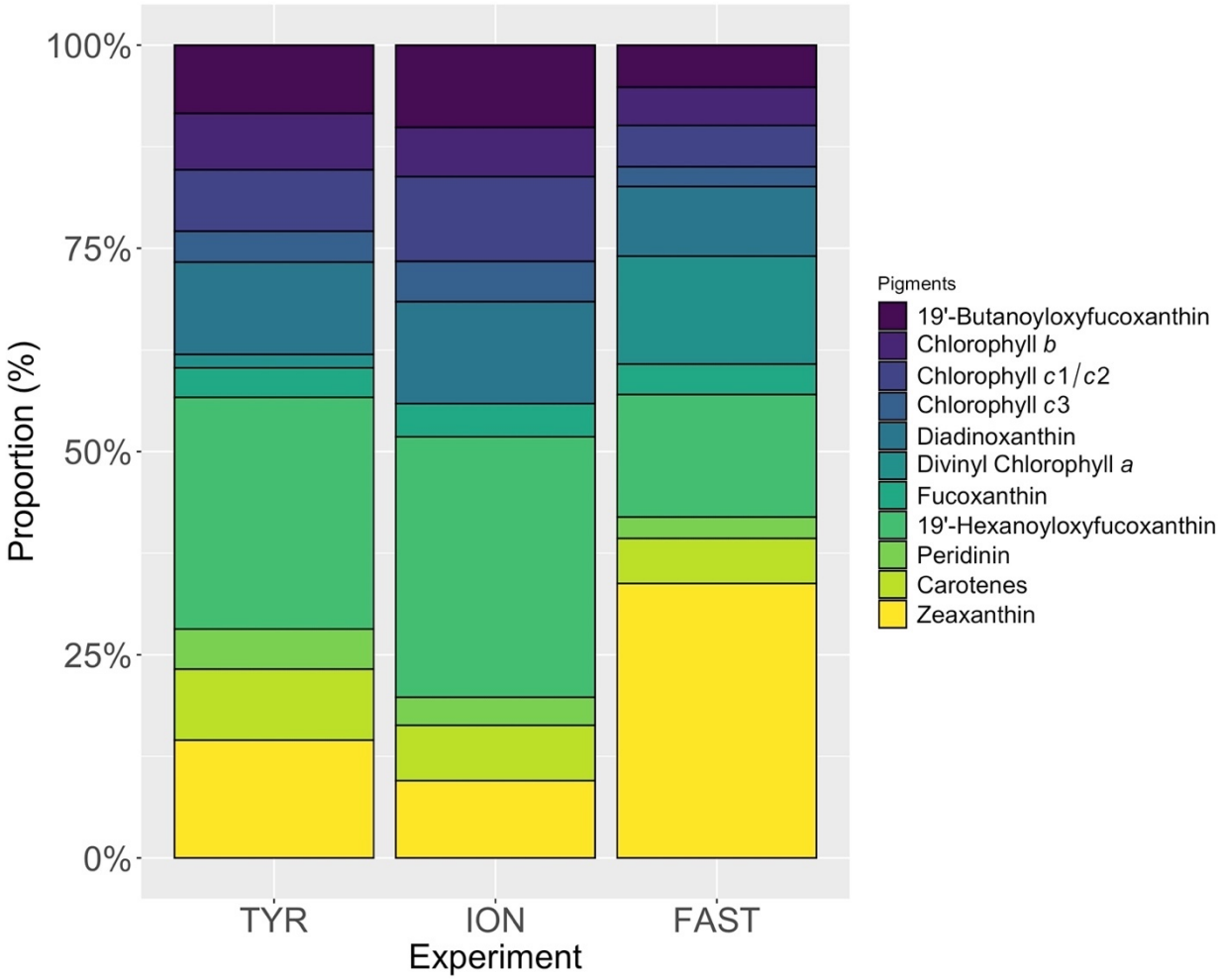
100%
75%
50%
25%
0%
Proportion (%)
TYR
ION
FAST
Experiment
Pigments
19'-Butanoyloxyfucoxanthin
Chlorophyll b
Chlorophyll c1/c2
Chlorophyll c3
Diadinoxanthin
Divinyl Chlorophyll a
Fucoxanthin
19'-Hexanoyloxyfucoxanthin
Peridinin
Carotenes
Zeaxanthin

Fig. 3.

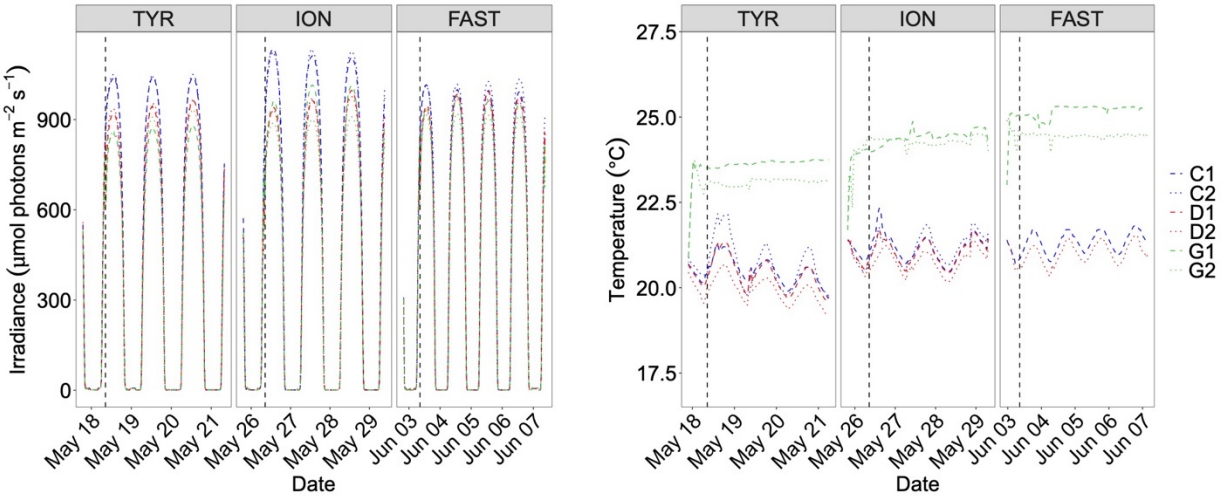
TYR
ION
FAST
Irradiance (µmol photons m^{-2} s^{-1})
0
300
600
900
May 18
May 19
May 20
May 21
May 26
May 27
May 28
May 29
Jun 03
Jun 04
Jun 05
Jun 06
Jun 07
Date
Temperature (°C)
17.5
20.0
22.5
25.0
27.5
C1
C2
D1
D2
G1
G2

Fig. 4.

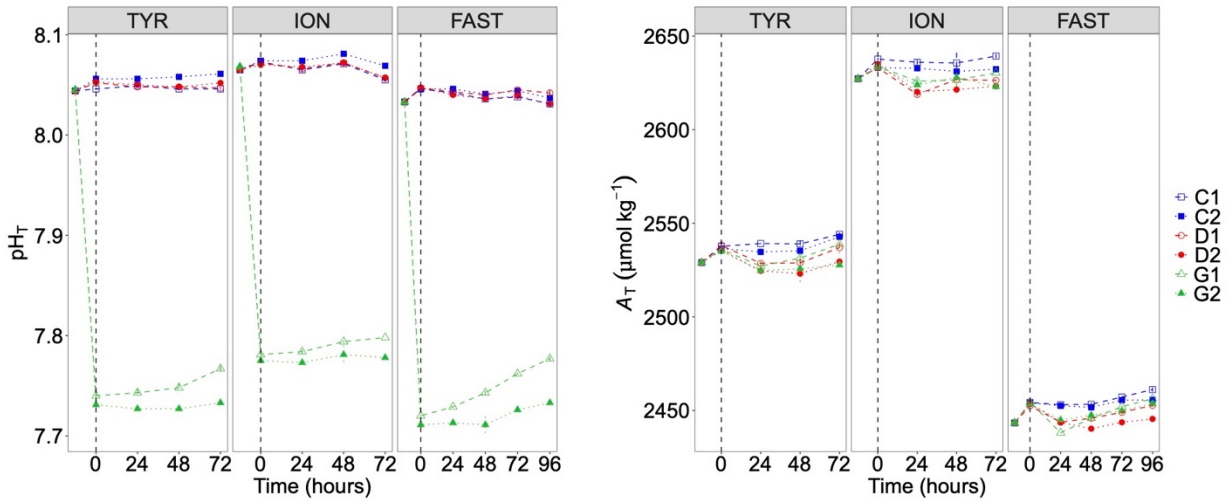
TYR
ION
FAST
8.1
8.0
7.9
7.8
7.7
pH_T
0 24 48 72
0 24 48 72
0 24 48 72 96
Time (hours)
2650
2600
2550
2500
2450
A_T (µmol kg^-1)
0 24 48 72
0 24 48 72
0 24 48 72 96
Time (hours)
C1
C2
D1
D2
G1
G2

Fig. 5.

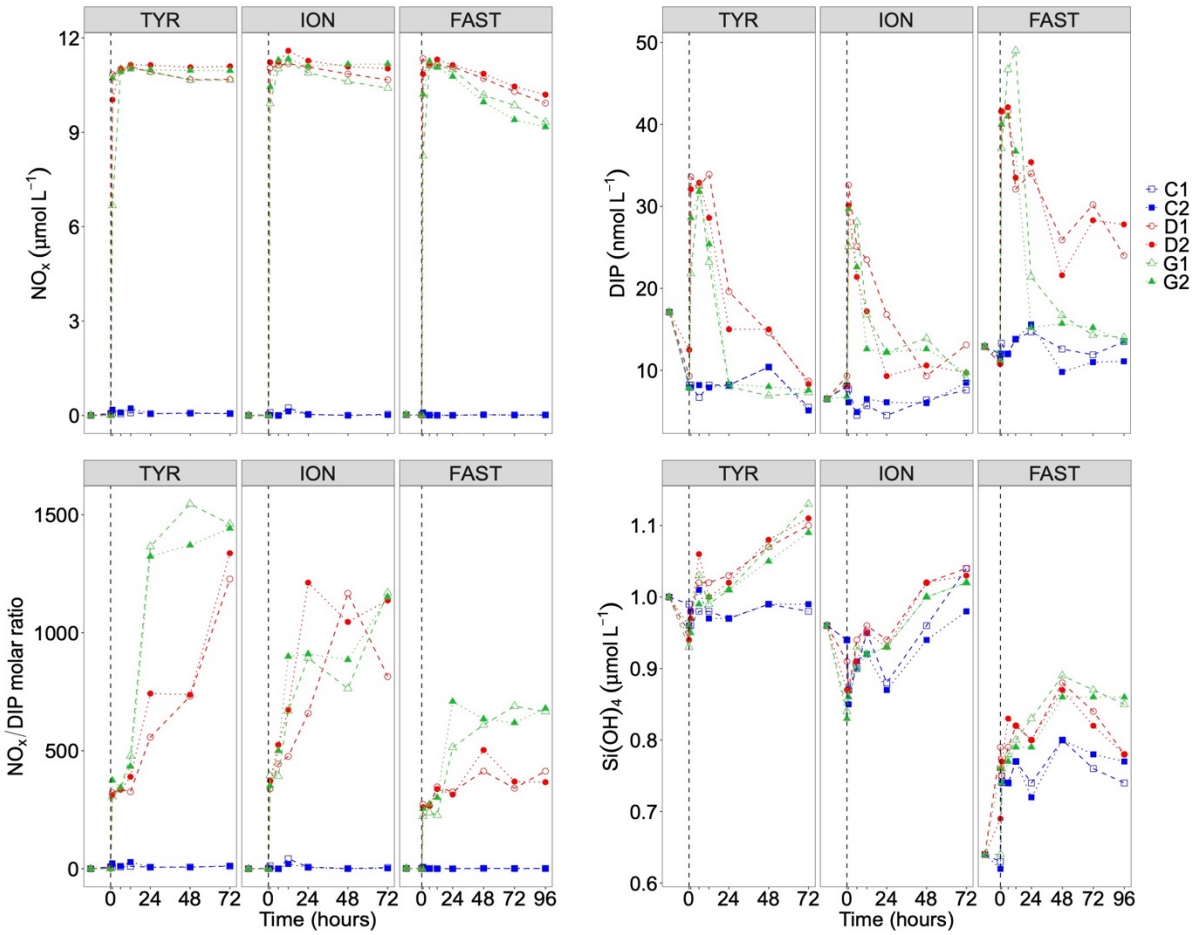
TYR
ION
FAST
NOx (µmol L-1)
DIP (nmol L-1)
NOx/DIP molar ratio
Si(OH)4 (µmol L-1)
Time (hours)
C1
C2
D1
D2
G1
G2

Fig. 6.

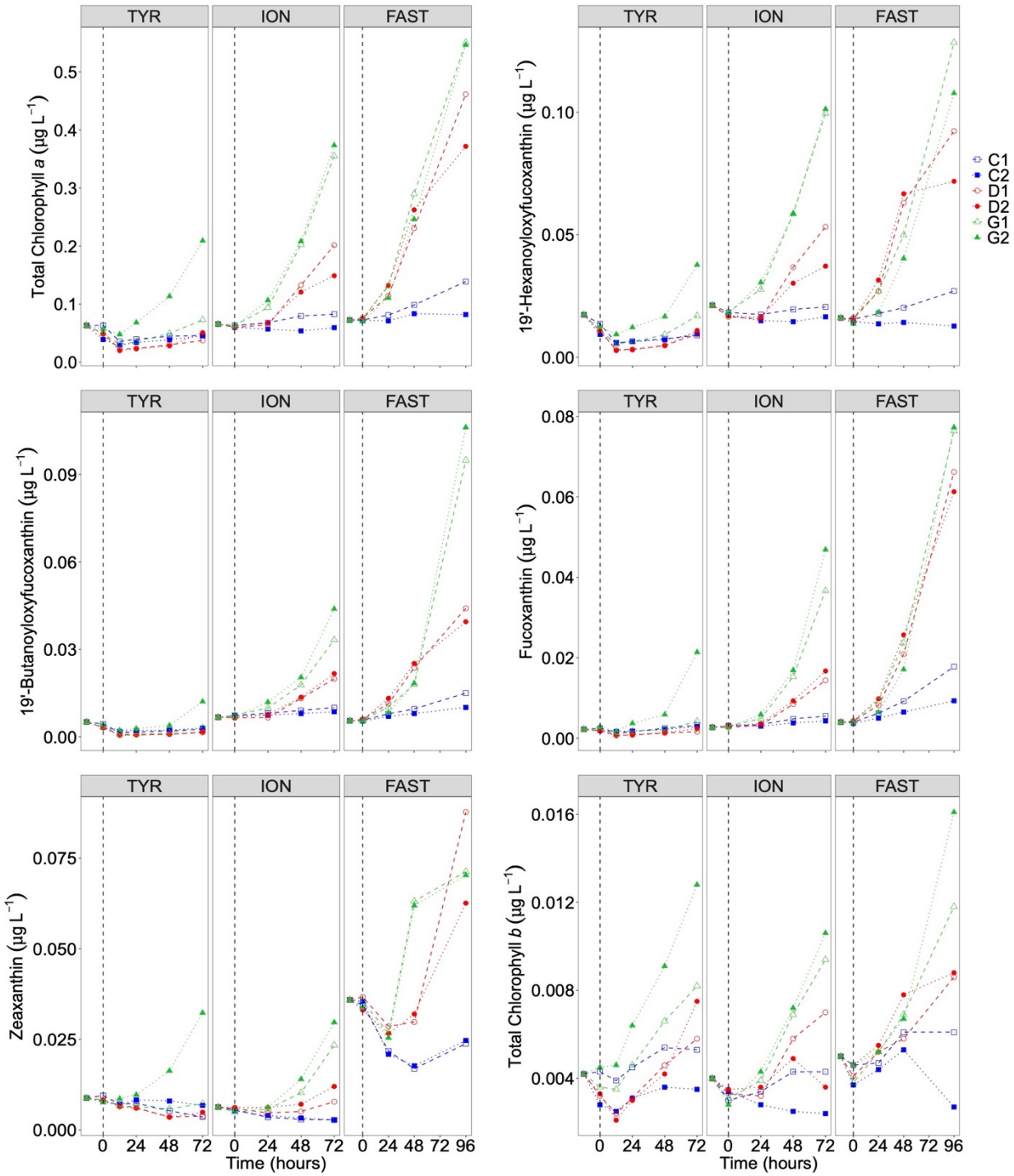
TYR
ION
FAST
Total Chlorophyll a (µg L⁻¹)
19'-Hexanoyloxyfucoxanthin (µg L⁻¹)
19'-Butanoyloxyfucoxanthin (µg L⁻¹)
Fucoxanthin (µg L⁻¹)
Zeaxanthin (µg L⁻¹)
Total Chlorophyll b (µg L⁻¹)
Time (hours)
C1
C2
D1
D2
G1
G2

Fig. 7.

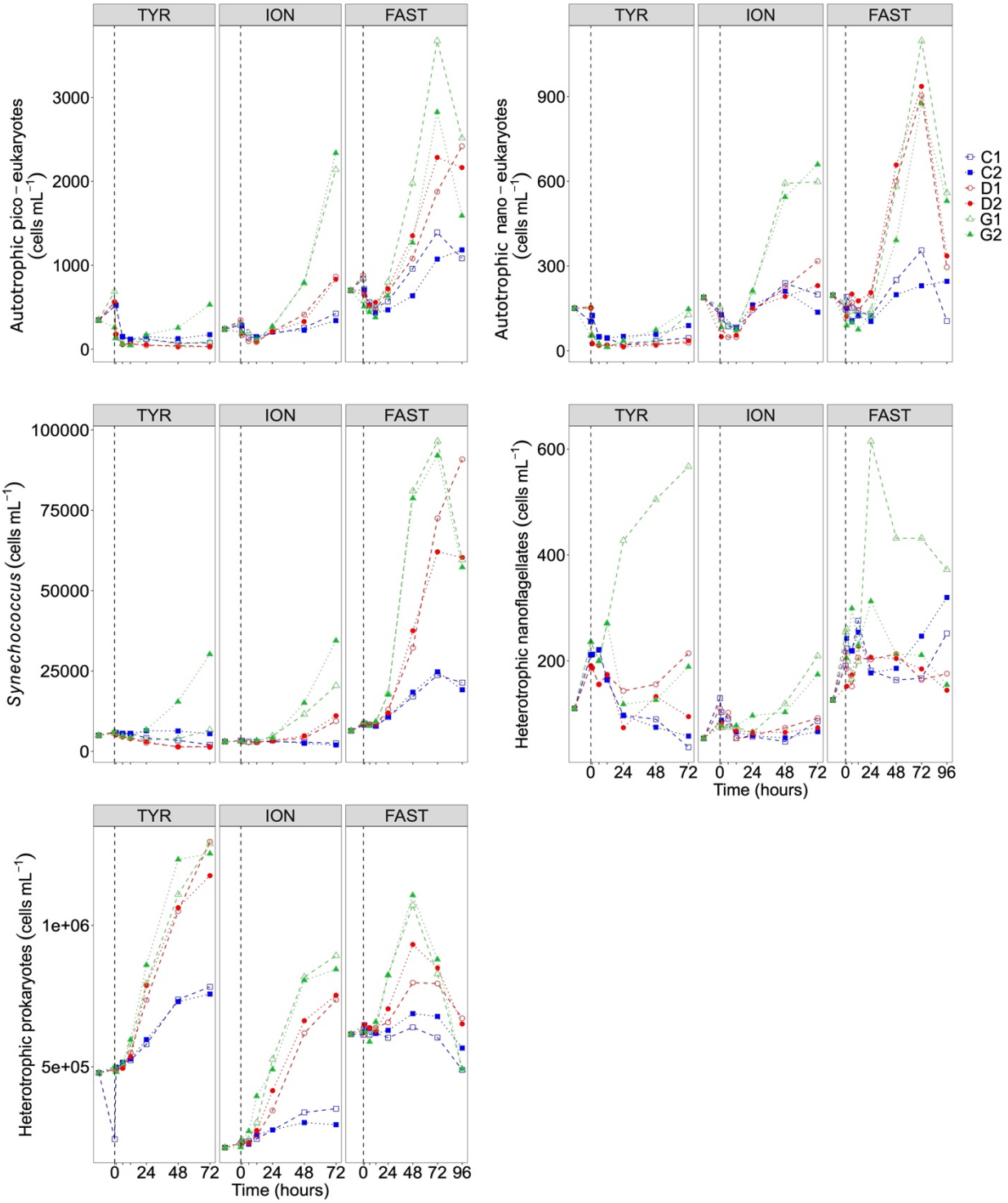
TYR
ION
FAST
Autotrophic pico – eukaryotes (cells mL^{-1})
Autotrophic nano – eukaryotes (cells mL^{-1})
Synechococcus (cells mL^{-1})
Heterotrophic nanoflagellates (cells mL^{-1})
Heterotrophic prokaryotes (cells mL^{-1})
Time (hours)
C1
C2
D1
D2
G1
G2

Fig. 8.

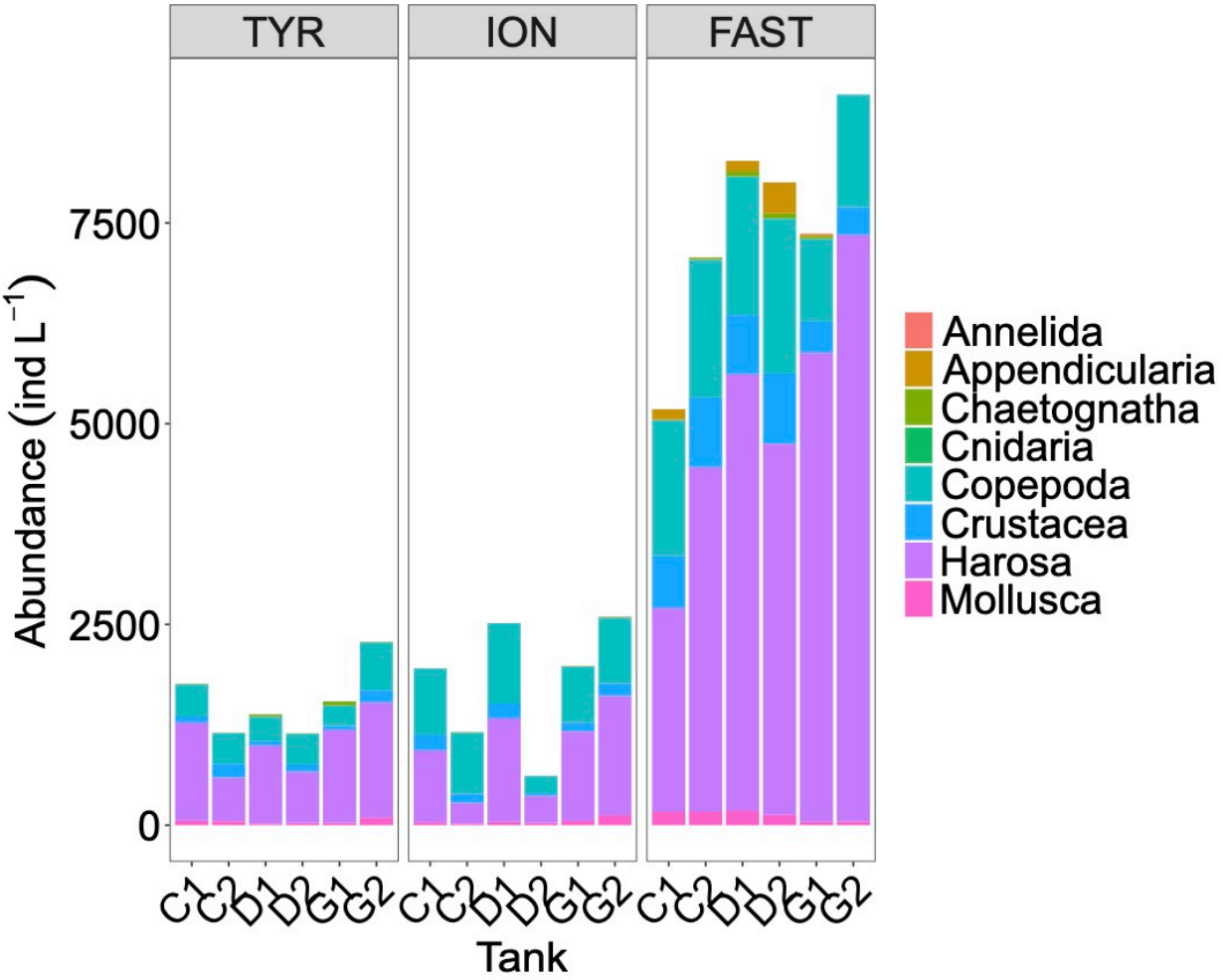
TYR
ION
FAST
7500
5000
2500
0
Abundance (ind L^{-1})
Tank
Annelida
Appendicularia
Chaetognatha
Cnidaria
Copepoda
Crustacea
Harosa
Mollusca

Fig. 9.

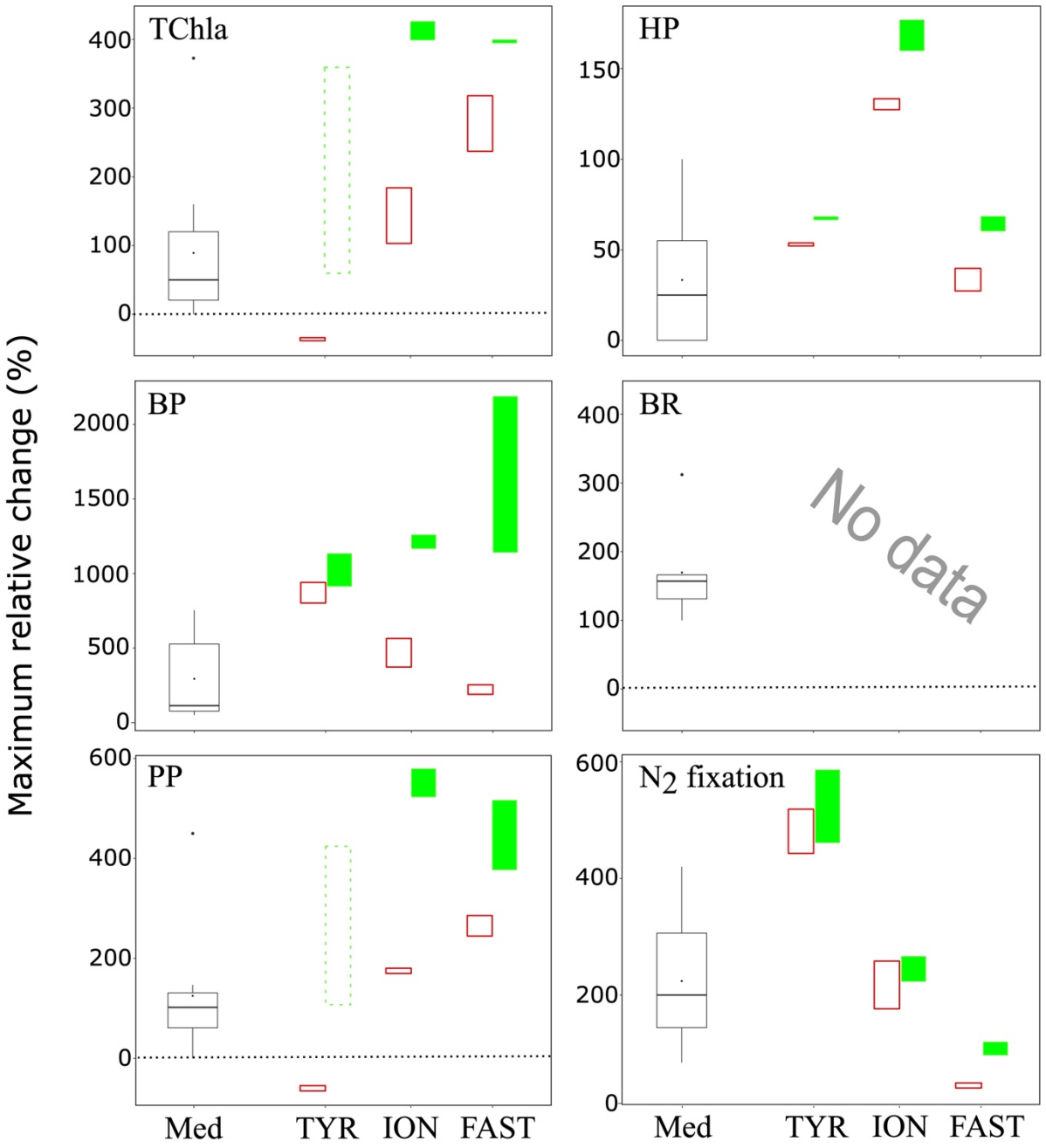
Maximum relative change (%)
TChla
HP
BP
BR
No data
PP
N2 fixation
Med
TYR
ION
FAST

Fig. 10.